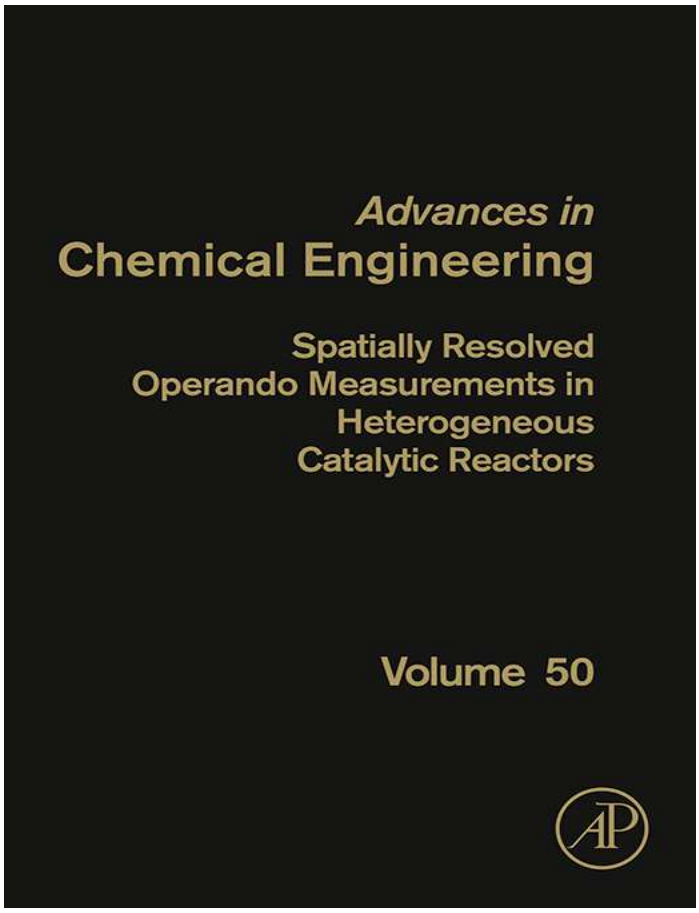

From Alessandra Beretta, Gianpiero Groppi, Andrea Carrera and Alessandro Donazzi, Analysis of the Impact of Gas-Phase Chemistry in Adiabatic CPO Reactors by Axially Resolved Measurements. In: Anthony G. Dixon and Olaf Deutschmann, editors, *Advances in Chemical Engineering, Vol. 50*, Burlington: Academic Press, 2017, pp. 161-201.
ISBN: 978-0-12-812589-2

CHAPTER FOUR

Analysis of the Impact of Gas-Phase Chemistry in Adiabatic CPO Reactors by Axially Resolved Measurements

Alessandra Beretta[1], **Gianpiero Groppi, Andrea Carrera, Alessandro Donazzi**

LCCP—Laboratory of Catalysis and Catalytic Processes, Dipartimento di Energia, Politecnico di Milano, Milano, Italy

[1]Corresponding author: e-mail address: alessandra.beretta@polimi.it

Contents

Abstract

This chapter focuses on the contribution that the in situ probing of temperature and concentration profiles in high-temperature and short contact time partial oxidation processes has given to the understanding of the interplay between homogeneous and heterogeneous chemistry. Experimental evidence was collected in our laboratory on the gas-phase conversion of C_{2+} fuels in adiabatic CPO reformers. The formation of short-chain hydrocarbons can promote the syngas performance, since the fed fuel is partly transformed into highly reactive species which further react on the surface producing CO and H_2; however, short olefins are soot/coke precursors and the surface condensation or breakthrough of such species is highly undesired. The experience from

Advances in Chemical Engineering, Volume 50
ISSN 0065-2377
https://doi.org/10.1016/bs.ache.2017.09.001

CPO reactors and other similar processes allows to understand the effects that pressure and dilution, the nature of the fuel and of the catalyst, and heat dispersions across the reactor have on the final fate of the cracking intermediates. The possibility to tune the relative contributions of the gas-phase and the surface chemistry in order to limit the catalyst hot spot temperature is also discussed.

1. INTRODUCTION

Small-scale fuel processing has been studied in the last 15–20 years as one of the possible solutions for the decentralized and the on-board production of H_2 for H_2-fuelled vehicles using fossil fuels (Armor, 1999; Basini, 2005; Villegas et al., 2014; Xu et al., 2013). Originally, hydrocarbon reforming represented a key factor of the so-called hydrogen economy. Nowadays, while the perspective of fuel cells-driven vehicles becomes more and more close, the use of fossil fuels for H_2-refuelling stations is conceived as a transition stage necessary for supporting the birth of a H_2 market before the development of technologies based on renewable energy (e.g., H_2 production by water electrolysis powered by solar energy or wind energy) is complete.

Additionally, the interest for developing compact small-scale processors using fossil or biofuels remains lively for several potential applications, from stationary combined heat and power systems (Galvagno et al., 2013; Kaltschmitt and Deutschmann, 2012; Kolb et al., 2007), to on-board H_2 generation for H_2-enhanced IC engines (Galloni and Minutillo, 2007; Mehra et al., 2017; Soberanis and Fernandez, 2010), regeneration of NO_x traps on diesel vehicles (Mundschau et al., 2010), and fuelling of SOFC- or HTPEM-based auxiliary power units for cars, ships, and aircrafts (Fabiano et al., 2016; Pasel et al., 2004; Samsun et al., 2017).

The catalytic partial oxidation of hydrocarbons presents several potential advantages, highly attractive at this scope: easy scalability, flexibility to fuels, fast dynamic response, and, most importantly, autothermal character which greatly simplifies the processing system due to the absence of exo- and endothermic compartments. The autothermal operation of the CPO reformers has been proven at the lab scale in the so-called short contact time reactors, pioneered by Schmidt and his group at Minnesota, consisting of foam or honeycomb supports coated with a metal-containing washcoat (Hickman and Schmidt, 1992, 1993; Hickman et al., 1993). Those original results have been largely confirmed over the years, and Rh-supported catalysts have

become the materials of choice for several proven proof-of-concept and demonstration units based on reforming or autothermal reforming of gaseous and liquid fuels because of high activity and reduced tendency to coking (Basile et al., 2003; Pasel et al., 2016; Specchia et al., 2012; Vita et al., 2017).

Although a direct partial oxidation route to CO and H_2 has been claimed in early studies, the kinetics of the CPO of several hydrocarbons (methane has been mostly studied, but also higher hydrocarbons) over Rh/Al_2O_3 and other catalysts can be well explained by a reaction scheme, consisting on one side of the consumption of O_2 in the deep oxidation of the fuel and the postcombustion of CO and H_2, and on the other side of the steam reforming of the hydrocarbon to CO and H_2; WGS (water–gas shift), RWGS (reverse water–gas shift), and CO_X methanation can then affect the syngas composition, depending on the temperature and chemical potential of the reacting mixture. The relative rate of gas–solid fluxes and surface reactions determines the dominant chemical pathways and the product distribution; in fact, in a chemically controlled regime, deep oxidation is the primary reaction of the fuel (thus producing CO_2 and H_2O) and syngas is produced only consecutively to the complete conversion of O_2, while under a diffusion-controlled regime (where the concentration of O_2 at the wall is zero) steam reforming is active even in the presence of O_2 in the gas phase and is fully responsible for the fuel conversion, while postcombustions (mostly of H_2) are responsible for O_2 conversion (Maestri et al., 2009).

Under the operating conditions of the real application (adiabatic reactor, absence of feed dilution, wash-coated structured catalysts, millisecond contact times, gas–solid mass, and heat transfer limitations) the oxidation/reforming scheme results in the reaching of very high temperatures at the very entrance of the reactor. This turns out to be the inherent weakness of the CPO process, since high temperatures can cause catalyst sintering, activity loss, and reactor instability due to an autocatalytic deactivation process, resulting in a progressive heating of the system (Beretta et al., 2009).

Thus, a very accurate characterization of the temperature distribution across the reactor and especially at the entrance, as well as a detailed characterization of the chemical processes which determine the temperature evolution is extremely important.

The development of axially resolved sampling techniques has largely contributed to finely monitor the axial profiles of temperature and composition in short contact time CPO reactors (Morgan et al., 2016). It must be emphasized that in CPO reactors the peak of temperature and of reaction rates extinguishes within few millimeters from the monolith entrance; thus,

an extremely high resolution has been necessary to disclose the sharpness of temperature and concentration gradients. In our laboratory, these techniques have been applied to study the CPO of light hydrocarbons (methane and propane) and liquid hydrocarbons (iso- and normal octanes) over Rh. The information gained has supported the development and validation of a mathematical model of the adiabatic reactor that implements the reaction schemes derived from the independent kinetic investigations. We strongly believe in the need of a strict interplay between the operando investigation and the development of engineering tools of simulations, necessary on one side to rationalize the observed phenomenon (e.g., by understanding relative importance of reaction rate vs heat and mass transfer rates) and on the other side to develop improved solutions that can lead to the final application. In this respect, a very interesting phenomenon revealed by the internal probing of the CPO reactor has been the formation of short-chain hydrocarbons, which can hardly detected at the reactor outlet; the observation prompted the development of a more comprehensive reactor model incorporating both the heterogenous chemistry and the homogeneous chemistry, which in turn provided new elements for the reaction engineering analysis of the process.

In this chapter, we illustrate the phenomenology of the CPO process as it results from the in situ probing of temperature and concentration for various fuels; we then discuss the interpretation of the observed trends based on a modeling analysis. The understanding of the interaction between radical and surface reactions and an engineering analysis of the effect of operating parameters on such interaction offered additional tools for the optimal design of the CPO reformer, where the key issue is the minimization of the inlet hot spot temperature.

Finally, we discuss how the learning gained from the CPO of C_{2+} hydrocarbons can provide a key for the interpretation of the performances observed in similar high temperatures and fuel-rich oxidation processes (e.g., methane oxidative coupling (MOC), ethane oxidative dehydrogenation (ODH) to ethylene, ethanol partial oxidation).

2. APPLICATION OF THE SPATIALLY RESOLVED SAMPLING TECHNIQUE TO THE CPO OF C_{2+} HYDROCARBONS

This section presents the results obtained in our laboratory by the application of the sampling technique to the investigation of temperature

and concentration profiles in the CPO of propane and the CPO of octane isomers over Rh. Experimental details are provided first.

2.1 Experimental Methods

2.1.1 Catalyst

The CPO tests were performed over a 2 wt% $Rh/\alpha\text{-}Al_2O_3$ catalyst supported onto 400 cpsi cordierite honeycombs. The catalyst was prepared by dry impregnation of the $\alpha\text{-}Al_2O_3$ support (10 m^2/g surface area by BET measurement) with an aqueous solution of $Rh(NO_3)_3$. Following a standard procedure, the catalyst was deposited over the honeycomb support by dip-coating and blowing-off of the slurry obtained from the catalyst powders. Adhesion of the deposited layer was achieved by subsequent drying at 280°C in an oven for 15 min. The catalyst load (~600–800 mg for monolith lengths of 2.5–3.5 cm) was estimated by weight difference before and after coating the monolith. The washcoat thickness (15–20 μm) was then calculated assuming a density of the catalyst layer of 1.38 g/cm^3. The final void fraction of the coated monolith varied in between 0.70 and 0.75.

2.1.2 Apparatus and Operating Conditions

The CPO experiments were carried out in a lab-scale testing rig placed under a fume hood for safety reasons. A diagram of the apparatus is presented in Fig. 1. Three lines fed gaseous reactants (air, CH_4 or C_3H_8, N_2), and one fed liquid fuels to the reactor. Gas flows were regulated by Brooks 5850S thermal mass flow controllers. A Gilson Minipuls 3 peristaltic pump delivered the liquid fuel (stocked in a 250 mL burette) into an evaporator, which consisted of a 40-cm-long ½ inch pipe, filled with quartz spheres (3 mm OD), heated by an annular Carbolite oven at a set point temperature of 170°C. Dilution nitrogen was fed to the evaporator, in order to ensure complete octane evaporation. In octane CPO tests, air is preheated as well, using two Watlow Starflow heating cartridges. Instead, CPO tests with light hydrocarbons were typically performed without any preheating of reactants.

Fuel and air were mixed in a Sulzer static mixer, placed immediately before the reactor. A K-type thermocouple was placed after the static mixer, in order to measure the reactants' temperature.

The reactor (Fig. 2) consisted of a stainless steel tube, externally insulated by wrapping a thick pad of quartz wool. To prevent C formation, a quartz liner was used for hosting the catalytic monolith in the reactor. Within this liner, the catalytic monolith was placed in between two inert blank monoliths, kept at a distance of ~1 cm, which acted as heat shields. This choice

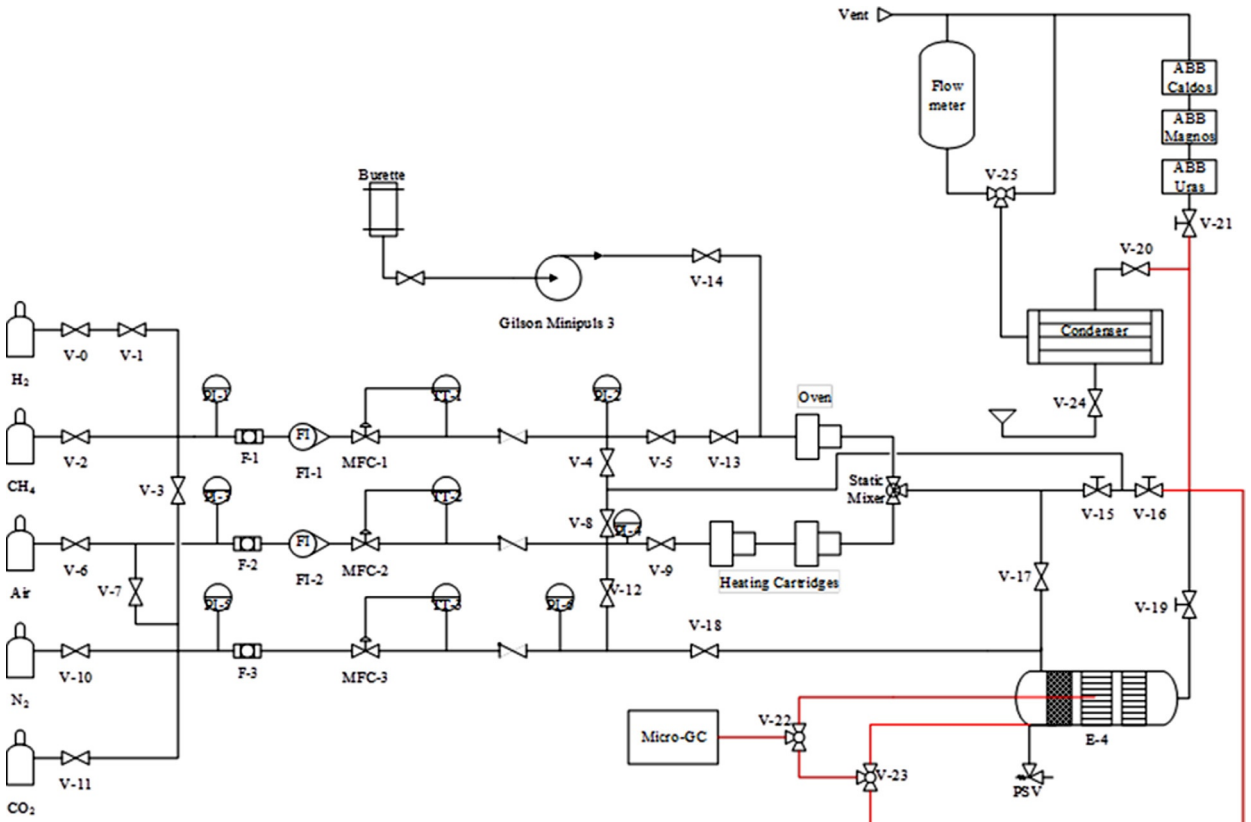

Fig. 1 P&I diagram of the testing rig used in this work. Heated lines are colored in *red*.

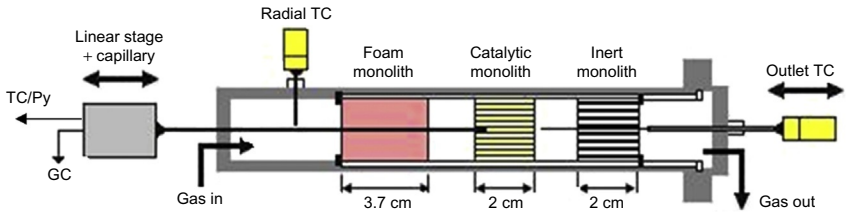

Fig. 2 Simplified scheme of the configuration of the adiabatic reactor. *Adapted from Carrera A, Pelucchi M, Stagni A, Beretta A, Groppi G, et al: Catalytic partial oxidation of n-octane and iso-octane: experimental and modeling results,* Int J Hydrogen Energy, *2017, https://doi.org/10.1016/j.ijhydene.2017.08.020, with permission from Elsevier.*

increased the radiant heat dissipation at the edges of the catalytic monolith, thus preserving it from excessive heating, especially in the inlet portion (Livio et al., 2011).

The setup of the reactor was designed to carry out spatially resolved measurements up to 4 bar. The sealing system was improved by addition of a guard filled with high vacuum grease (Dow Corning), which allowed to move the capillary and to avoid gas leakage. The pressure of the reactor was measured at the inlet and was regulated with a control valve at the outlet.

For the measurement of the spatially resolved concentration profile of the gas species, a deactivated fused silica capillary (O.D. = 350 μm, I.D. = 200 μm) was inserted into the central channel of the honeycomb and externally connected to a loop purposely designed for tests under pressure. The sampled flow (2 Ncc/min) was carefully controlled by connecting the capillary to a regulation valve. After this valve, the sampled flow was admitted to an empty volume connected to a micro-GC (Agilent 3000). For the spatially resolved measurements of temperature, the reactor was equipped with a K-type thermocouple (250 μm O.D.) and a narrow band infrared pyrometer (Impac Infrared, IGA 5-LO) connected to an optical fiber (300 μm core diameter, 330 μm O.D.). A larger capillary (O.D. = 500 μm) sealed at one end was used to move the optical fiber and the thermocouple. The thermocouple measurements were taken as representative of the temperature of the gas phase, whereas the measurements of the pyrometer were representative of the temperature of the catalyst surface (Donazzi et al., 2011a).

A micro gas chromatograph analyzed the gas streams by two modules, each equipped with a TCD detector: a Molecular Sieve Column (10 m length), with PLOT U precolumn (3 m length), using Ar as carrier gas, and a PLOT U column (6 m length), using He as carrier gas. Column A worked at 70°C, thus separating H_2, N_2, O_2, CH_4, and CO. In

experiments with liquid fuels, Column B was operated at two different temperatures, namely, 160°C and 60°C; the analysis at the highest temperature was performed to quantify iso-octane and *n*-octane concentrations, while the lowest temperature analysis separated light hydrocarbon species. Continuous gas analyzers also collected integral data at the reactor outlet.

The CPO tests were performed at 5–10 NL/min. Pressure was varied in between 1 and 4 bar for the C_3H_8 CPO tests, while atmospheric pressure was maintained in the campaign with octane fuels. Before each test, the catalyst was preheated with a 6% v/v hydrogen and 3% v/v oxygen in nitrogen mixture, with a flow rate of 5 NL/min. The catalytic combustion of hydrogen preheated the catalyst. As soon as the temperature measured by the rear thermocouple reached 200°C in case of propane or octane CPO or 240°C in case of methane CPO, the inlet mixture of the reactor was switched to the feed mixture for the desired CPO test. The results have been collected in steady-state conditions, at least 30′ after reaction ignition.

In the case of C_3H_8 CPO, the experiments were performed with propane/air mixtures with an O_2/C ratio between 0.56 and 0.60.

In the case of the liquid fuels, CPO tests were performed at varying dilution; most of the experiments were obtained at 2% C_8H_{18} in the feed with a C/O ratio in between 0.83 and 0.90, which corresponds to a nitrogen dilution from 52% to 56%. Additional experiments were performed at decreasing dilution to verify the severity of the thermal behavior for a nondiluted fuel-rich mixture. The reactants were preheated at a temperature of 85°C, in order to avoid octane condensation.

2.2 Mathematical Model of the Reactor and Kinetic Scheme

The experiments were analyzed by a 1D, adiabatic, heterogeneous model of the honeycomb reactor, assuming single-channel approximation, i.e., all the channels are representative of the reactor performance. The model consists of mass and enthalpy balances for the gas phase and solid phase. The model also includes axial convection and diffusion terms, solid-phase conduction, and gas–solid transport terms, estimated with correlations for laminar flow in square channels. Heat conduction in the solid was taken into account with an effective axial thermal conductivity coefficient, corrected by addition of the radiation contribution. The complete set of the equations is reported in Table 1.

The model includes kinetic schemes for the solid phase and gas phase. The heterogeneous kinetic scheme was proposed in previous works starting from the development of a C_1 kinetic scheme (Donazzi et al., 2008a,b), and

Table 1 Model Equations

Gas phase

Mass balance

$$\frac{\partial \omega_i}{\partial t} = -\frac{G}{\rho_g \varepsilon}\frac{\partial \omega_i}{\partial z} - \frac{a_v}{\varepsilon} k_{\mathrm{mat},i}(\omega_i - \omega_{\mathrm{wall},i}) + \frac{1}{\varepsilon}\frac{\partial}{\partial z}\left(\mathfrak{D}_i \frac{\partial \omega_i}{\partial z}\right) + \frac{MW_i}{\rho_g}\sum_{j=1}^{NR_s} \upsilon_{i,j} r_j^{\mathrm{hom}} \quad (1)$$

Enthalpy balance

$$\frac{\partial T_g}{\partial t} = -\frac{G}{\rho_g \varepsilon}\frac{\partial T_g}{\partial z} - \frac{a_v h\left(T_g - T_s\right)}{\varepsilon \rho_g \hat{c}_{p,g}} + \frac{1}{\varepsilon \rho_g \hat{c}_{p,g}}\frac{\partial}{\partial z}\left(k_g \frac{\partial T_g}{\partial z}\right) - \frac{1}{\rho_g \hat{c}_{p,g}}\sum_{j=1}^{NR_s} \Delta H_{r,j} r_j^{\mathrm{hom}} \quad (2)$$

Solid phase

Mass balance

$$0 = a_v \rho_g k_{\mathrm{mat},i}(\omega_i - \omega_{\mathrm{wall},i}) + MW_i \rho_w \alpha \sum_{j=1}^{NR_s} \upsilon_{i,j} r_j^{\mathrm{het}} \quad (3)$$

Enthalpy balance

$$\frac{\partial T_s}{\partial t} = \frac{a_v h\left(T_g - T_s\right)}{(1-\varepsilon)\rho_s \hat{c}_{p,s}} + \frac{\frac{\partial}{\partial z}\left(k_{ax}^{\mathrm{eff}} \frac{\partial T_s}{\partial z}\right)}{(1-\varepsilon)\rho_s \hat{c}_{p,s}} - \frac{\alpha \rho_w}{(1-\varepsilon)\rho_s \hat{c}_{p,s}} \sum_{j=1}^{NR_s} \Delta H_{r,j} r_j^{\mathrm{het}} \quad (4)$$

Boundary conditions

Reactor inlet ($z = -0.5$ cm, any t)

$$\left.\frac{\partial T_s}{\partial z}\right|_{z=-0.5\,\mathrm{cm}} = 0 \quad (5)$$

Catalyst inlet ($z = 0$, any t)

$$\omega_i|_{z=0} = \omega_{i,\,\mathrm{feed}} + \left.\frac{D_i}{v}\frac{\partial \omega_i}{\partial z}\right|_{z=0}; \; T_g|_{z=0} = T_{\mathrm{feed}} + \left.\frac{k_g}{v \rho_g \hat{c}_{p,g}}\frac{\partial T_g}{\partial z}\right|_{z=0} \quad (6)$$

Catalyst outlet ($z = L$, any t)

$$\left.\frac{\partial \omega_i}{\partial z}\right|_{z=L} = 0; \; \left.\frac{\partial T_s}{\partial z}\right|_{z=L} = 0 \quad (7)$$

Initial conditions ($t = 0$, any z)

$$\omega_i(z, 0) = 0; T_g(z, 0) = T_{\mathrm{feed}}; T_s(z, 0) = 650°\mathrm{C} \quad (8)$$

progressively extended by the addition of lumped reactions for the oxidation and steam reforming of propane, iso-octane, and *n*-octane (Carrera et al., 2017a,b; Pagani et al., 2012). The whole scheme includes then the WGS reaction and its reverse RWGS, a CO methanation route, and the post-combustions of CO and H_2. The kinetic dependences for each reaction were studied over the years by dedicated experiments, where single reactions were "isolated" from the global CPO process with dedicated experiments and kinetic analysis. The whole scheme is reported in Table 2.

The kinetic scheme also incorporates the reaction of steam reforming of all the hydrocarbon species that are produced in the gas phase; these species include mainly propylene, ethylene, and ethane in the case of propane CPO, but include also several other C_4 and C_{4+} species in the CPO of the octanes. As discussed in a following section, this further extension of the heterogeneous kinetic scheme was a key assumption to adequately describe the observed phenomenology.

Gas-phase reactions were described according to the schemes proposed by Ranzi and coworkers (Carrera et al., 2017b; Pelucchi et al., 2014; Ranzi et al., 2012; Stagni et al., 2016).

The numerical analysis herein reported is fully predictive, with no parameter adjustment. The only input data of the calculations were the catalyst amount, the Rh load and dispersion, the geometrical parameters, and the physical properties of the honeycomb support.

2.3 Detection of Gas-Phase Products in the Autothermal CPO of Propane

It is first instructive to analyze the behavior of the propane/O_2 reacting system in isothermal activity tests, as those performed in annular reactor. Fig. 3 reports the results of experiments at the space velocity of 2×10^6 L(NTP)/kg_{cat}/h, with feed composition of 1% C_3H_8 and O_2/C ratio = 0.56 in N_2 dilution. These data have been fully analyzed elsewhere (Pagani et al., 2012), and we herein focus on the evidence that the evolution of the product distribution is very well explained by a kinetic scheme wherein CO_2 and H_2O are primary products of propane fuel-rich oxidation, while syngas is formed by a consecutive route of steam reforming and WGS; solid lines represent the prediction of a isothermal PFR model of the annular reactor incorporating the kinetic scheme reported in Table 2. Interestingly, CH_4 was also formed with a maximum (Fig. 3), coherently with the existence of a consecutive methanation reaction that approaches the thermodynamic equilibrium at high temperature. In other experiments at increasing flow rate,

Table 2 Heterogeneous Kinetic Scheme

Reaction	Rate$_i$ (mol g_{cat}^{-1} s^{-1})	$K_i^{873\,K}$ (mol atm^{-1} g_{cat}^{-1} s^{-1})	E_{ACT} (kJ mol^{-1})
i-C_8H_{18} total oxidation $i\text{-}C_8H_{18} + \frac{25}{2}O_2 \rightarrow 8CO_2 + 9H_2O$	$R_{Ox,i\text{-}C_8H_{18}} = \frac{k_{Ox,i\text{-}C_8} P_{i\text{-}C_8H_{18}}}{1 + K_{H_2O} P_{H_2O}} \sigma_{O_2}$	4.600E − 01	80.00
i-C_8H_{18} steam reforming $i\text{-}C_8H_{18} + 8H_2O \rightarrow 8CO + 17H_2$	$R_{SR,i\text{-}C_8H_{18}} = \frac{k_{SR,i\text{-}C_8} P_{i\text{-}C_8H_{18}}}{1 + K_{i\text{-}C_8H_{18}}^{poison} \frac{P_{i\text{-}C_8H_{18}}}{P_{H_2O}}} \cdot \left(1 - \eta_{i\text{-}C_8H_{18}}^{SR}\right) \cdot \sigma_{H_2O}$	7.500E − 02	69.00
n-C_8H_{18} total oxidation $C_8H_{18} + \frac{25}{2}O_2 \rightarrow 8CO_2 + 9H_2O$	$R_{Ox,n\text{-}C_8H_{18}} = \frac{k_{Ox,n\text{-}C_8} \cdot P_{n\text{-}C_8H_{18}}}{1 + K_{H_2O} P_{H_2O}} \cdot \sigma_{O_2}$	1.9E − 02	88
n-C_8H_{18} steam reforming $C_8H_{18} + 8H_2O \rightarrow 8CO + 17H_2$	$R_{SR,n\text{-}C_8H_{18}} = \frac{k_{SR,n\text{-}C_8} \cdot P_{n\text{-}C_8H_{18}}}{1 + K_{n\text{-}C_8H_{18}}^{poison} \frac{P_{i\text{-}C_8H_{18}}}{P_{H_2O}}} \cdot \left(1 - \eta_{n\text{-}C_8H_{18}}^{SR}\right) \cdot \sigma_{H_2O}$	7.5E − 02	69
C_3H_8 total oxidation $C_3H_8 + 5O_2 \rightarrow 3CO_2 + 4H_2O$	$R_{Ox,C_3H_8} = \frac{k_{Ox,C_3} P_{C_3H_8}}{1 + K_{H_2O} P_{H_2O}} \cdot \sigma_{O_2}$	2.500E − 01	80.00
C_3H_8 steam reforming $C_3H_8 + 3H_2O \leftrightarrow 3CO + 7H_2$	$R_{SR,C_3H_8} = \frac{k_{SR,C_3H_8} P_{C_3H_8}}{1 + K_{O_2} P_{O_2} + K_{CO} P_{CO}} \cdot \left(1 - \eta_{C_3H_8}^{SR}\right) \cdot \sigma_{H_2O}$	2.486E − 01	84.63
CH_4 total oxidation $CH_4 + 2O_2 \rightarrow CO_2 + 2H_2O$	$R_{Ox,CH_4} = \frac{k_{Ox,CH_4} P_{CH_4}}{1 + K_{H_2O}^{ads} p_{H_2O}} \cdot \sigma_{O_2}$	1.030E − 01	91.96
CH_4 steam reforming $CH_4 + H_2O \leftrightarrow CO + 3H_2$	$R_{SR,CH_4} = \frac{k_{SR,CH_4} P_{CH_4}}{1 + K_{O_2} P_{O_2} + K_{CO} P_{CO}} \cdot \left(1 - \eta_{CH_4}^{SR}\right) \cdot \sigma_{H_2O}$ $\eta_{CH_4}^{SR} < 1$	1.027E − 01	91.80
C_xH_y steam reforming $C_xH_y + xH_2O \rightarrow xCO + \left(\frac{y}{2} + x\right)H_2$	$r_{SR\,C_xH_y} = \frac{k_{SR\,C_xH_y} P_{C_xH_y} \left(1 - \eta_{SR\,C_xH_y}\right)}{1 + K_{CO} P_{CO} + K_{O_2} P_{O_2}} \sigma_{H_2O}$	2.486E − 01	84.63

Continued

Table 2 Heterogeneous Kinetic Scheme—cont'd

Reaction	Rate$_i$ (mol $g_{cat}^{-1}\,s^{-1}$)	K_i^{873K} (mol $atm^{-1}\,g_{cat}^{-1}\,s^{-1}$)	E_{ACT} (kJ mol^{-1})
Water–gas shift $CO + H_2O \leftrightarrow CO_2 + H_2$	$R_{WGS} = k_{WGS} P_{H_2O}(1-\eta_{WGS})\sigma_{CO}$ $\eta_{WGS} < 1$	6.831E − 03	74.83
Reverse water–gas shift $CO_2 + H_2 \leftrightarrow CO + H_2O$	$R_{RWGS} = k_{RWGS} P_{CO_2}(1-\eta_{RWGS})\sigma_{H_2}$ $\eta_{RWGS} < 1$	1.277E − 02	62.37
H_2 oxidation $H_2 + \frac{1}{2}O_2 \rightarrow H_2O$	$R_{OxH_2} = k_{OxH_2} P_{H_2} \sigma_{O_2}$	2.666E + 03	61.65
CO oxidation $CO + \frac{1}{2}O_2 \rightarrow CO_2$	$R_{OxCO} = k_{OxCO} P_{CO} \sigma_{O_2}$	1.937E + 01	76.07
CO methanation $CO + 3H_2 \leftrightarrow CH_4 + H_2O$	$R_{MetCO} = k_{MetCO} P_{H_2}(1-\eta_{MetCO})\sigma_{CO}$ $\eta_{MetCO} < 1$	1.200E − 03	88.02
$r_{\text{chemical reaction}} = r_{\text{chemical reaction}}\big\vert_{873\,K} \exp\left[-\frac{E_{att,\,r_j}}{R}\left(\frac{1}{T}-\frac{1}{873}\right)\right]$			

Surface Adsorption	K_i^{873K} (atm^{-1})	ΔH_{ADS} (kJ mol^{-1})
O_2	5.461E + 00	−72.83
CO	2.114E + 02	−37.15
H_2O	8.974E + 00	−57.48
C-poisoning i-C_8H_{18}	6.0E + 00	−26.0
C-poisoning n-C_8H_{18}	2.0E + 01	−35.5
$K_j = K_j^0 \exp\left[-\frac{\Delta H_{ADS}}{R}\left(\frac{1}{T}-\frac{1}{873.}\right)\right]$		

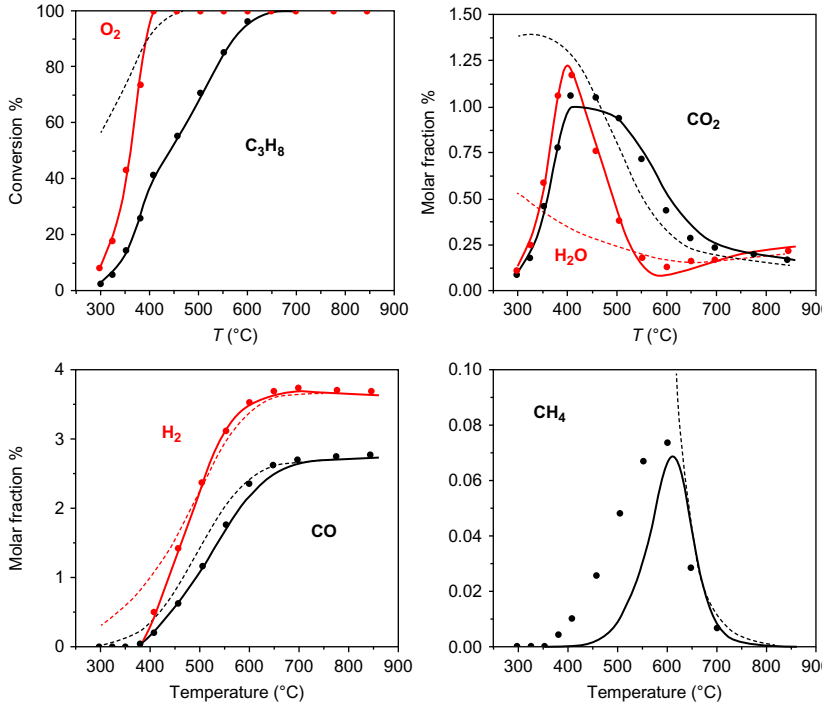

Fig. 3 Effect of temperature on reactants' and products' molar fractions. Experimental (*symbols*), calculated (*solid lines*), and equilibrium (*dashed line*) composition. GHSV = 2×10^6 L(NTP)/kg_{cat}/h. Feed composition: $C_3H_8 = 1\%$ (v/v), $O_2/C = 0.56$, N_2 to balance; atmospheric pressure. *Reprinted from Pagani D, Livio D, Donazzi A, et al: A kinetic analysis of the partial oxidation of C_3H_8 over a 2% Rh/Al_2O_3 catalyst in annular microreactor,* Catal Today *197:265–280, 2012, with permission from Elsevier.*

partially reported in Fig. 4, we observed that at the highest space velocities (4×10^6 and 6×10^6 L(NTP)/kg_{cat}/h) and above 700°C, small concentrations of methane, ethylene, and propylene were detected in the product mixture with an increasing trend with temperature (note that methane concentration grew against the thermodynamic equilibrium) and with flow rate; this clearly indicated that these species were produced in the gas phase by cracking reactions in the empty volume of the annular reactor downstream from the catalyst bed, and were not due to heterogeneous routes.

When the same process is performed in an adiabatic reactor, then the axial evolution of the process (consisting of highly exothermic and highly endothermic reactions) determines the interlinked evolution of reacting mixture composition and temperature.

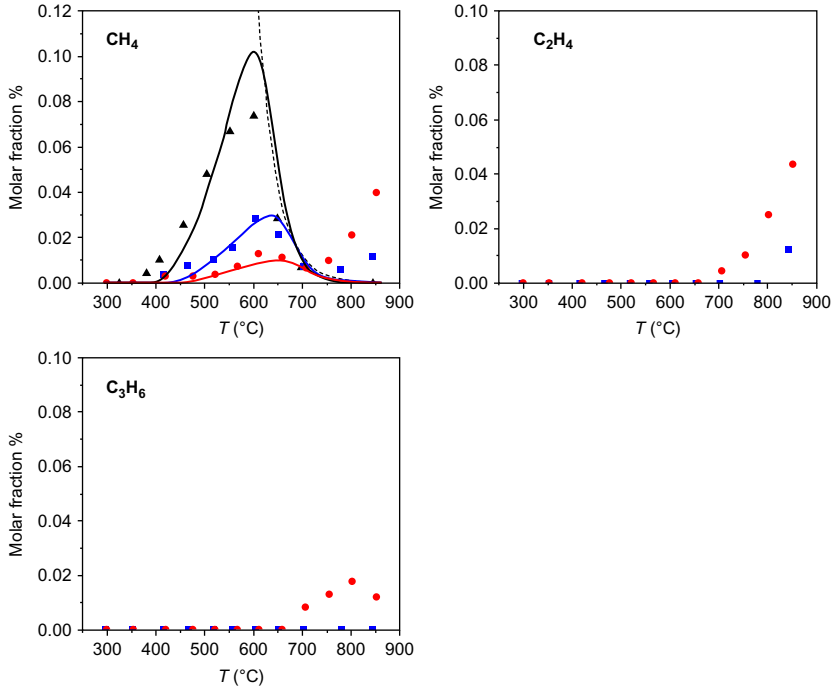

Fig. 4 Effect of GHSV and temperature on hydrocarbon side products' molar fractions. Experimental (*symbols*) fractions are reported. (▲) GHSV = 2×10^6 L(NTP)/kg_{cat}/h; (■) GHSV = 4×10^6 L(NTP)/kg_{cat}/h; (●) GHSV = 6×10^6 L(NTP)/kg_{cat}/h; (*dashed line*) equilibrium. Feed composition: C_3H_8 = 1% (v/v), O_2/C = 0.56, N_2 to balance; atmospheric pressure. *Reprinted from Pagani D, Livio D, Donazzi A, et al: A kinetic analysis of the partial oxidation of C_3H_8 over a 2% Rh/Al_2O_3 catalyst in annular microreactor,* Catal Today *197:265–280, 2012, with permission from Elsevier.*

Fig. 5 reports the results of a propane CPO experiment that was performed at 5 L(NTP)/min by feeding a propane/air mixture with O_2/C ratio of 0.56 (Donazzi et al., 2011a,b). In the first 5 mm of the honeycomb, a sharp drop of O_2 and C_3H_8 concentration was observed, accompanied by the formation of total oxidation products (CO_2 and H_2O) and partial oxidation products (H_2 and CO). Correspondingly, a hot spot formed on the catalyst surface (980°C, measured by the pyrometer) and a steep rise was observed in the gas temperature (up to 945°C, measured by the thermocouple). In line with the occurrence of the endothermic steam reforming reaction, the evolution of H_2O showed a maximum. As well, the temperatures of the solid surface and gas phase decreased toward the exit of the honeycomb. Qualitatively this is what our and other research groups have observed, also in the case of a CH_4-CPO experiment on Rh, and can be thus fully explained by

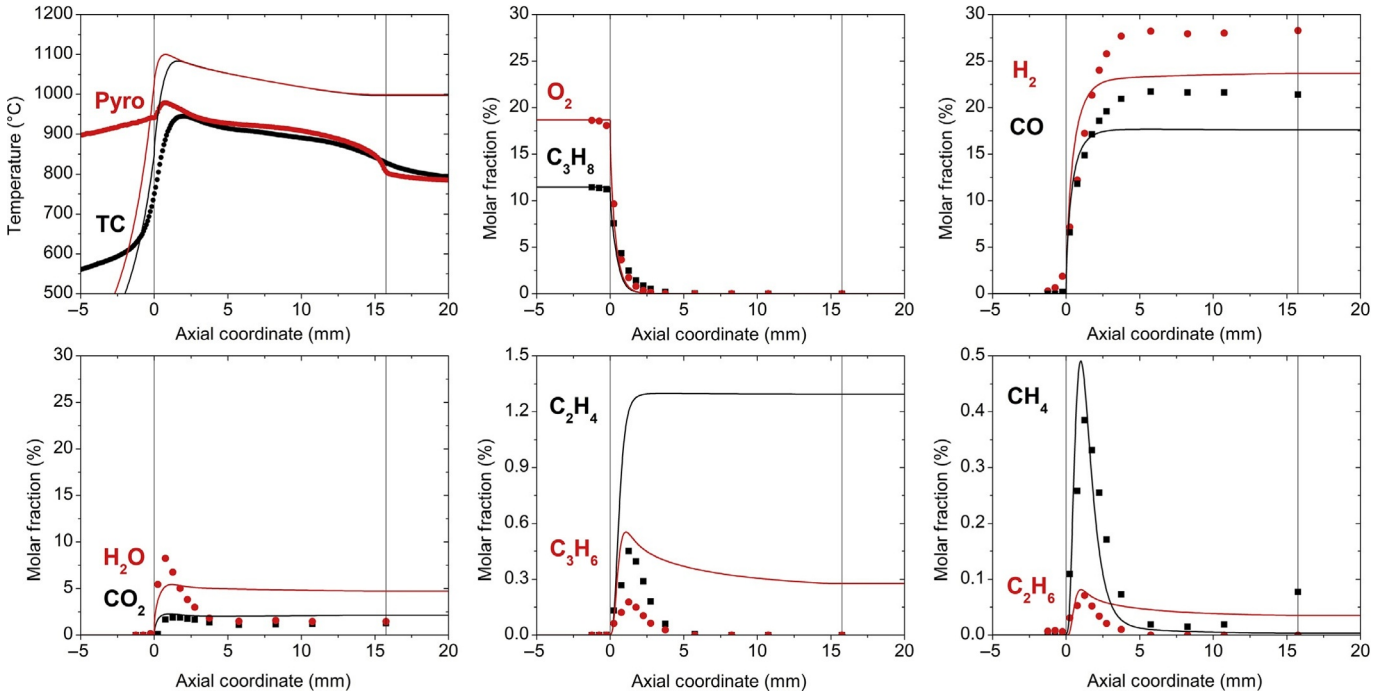

Fig. 5 Spatially resolved profiles of temperature and composition for a C_3H_8 CPO experiment. Flow rate = 5 L min^{-1} (STP), $P = 1$ atm. Feed: C_3H_8/air, $C_3H_8 = 11$ vol%, O/C = 1.12. Experimental results in *symbols*. *Solid lines* are calculations obtained by neglecting the steam reforming reactions of cracking products. *Reprinted from Donazzi A, Livio D, Maestri M, et al: Synergy of homogeneous and heterogeneous chemistry probed by in situ spatially resolved measurements of temperature and composition,* Angew Chem Int Ed *50:3943–3946, 2011, with permission from Wiley.*

the CPO chemistry on Rh. Thus, integral measurements (i.e., measurements of temperature and composition collected exclusively at the reactor outlet) would have suggested the unique existence of a heterogeneous process. However, the spatially resolved measurements revealed for the first time that several other species, such as C_2H_4, C_3H_6, and C_2H_6, were formed at the very reactor inlet and were then completely consumed before the ending section of the catalyst, passing through maxima.

We also observed a complex evolution of CH_4 that, similarly to C_2 and C_3 species, was initially formed and then consumed within the first half of the reactor, but tended to be formed again in the ending portion of the reactor. Since hydrocarbon species like olefins cannot be explained by the syngas formation paths on Rh, this experimental finding provided evidence of gas-phase chemistry.

In line with the interpretation of the experiments, the adiabatic model of the honeycomb monolith was first extended to include the detailed gas-phase chemistry from Ranzi et al. (2012), thus combining heterogeneous and homogeneous routes of propane activation. The model (solid lines in Fig. 5) could nicely describe the rapid evolution of the reacting mixture in the very first millimeters of the catalyst bed, namely: the rapid consumption of the reactants, the formation of deep and partial oxidation products, and the formation of methane, ethylene, propylene, and ethane. However, the evolution of temperature and product distribution along the rest of the monolith was not correctly described. The overall production of H_2 and CO was largely underestimated, while the outlet concentration of hydrocarbon species was greatly overestimated. Also, the predicted temperature profiles were much higher than observed.

Clearly, the simple description of the onset of a gas-phase chemistry (that under fuel-rich conditions favors the formation of short olefins) could not explain the outlet-selective formation of syngas. Only in the case of methane, the formation of a maximum was correctly described by the model; this was due to the fact that the gas-phase production of CH_4 at the reactor entrance "activated" the surface reaction of methane steam reforming, already present in the C_3 heterogeneous scheme.

The kinetic model was thus revised by incorporating in the heterogeneous scheme oxidation and steam reforming reactions for all the hydrocarbon species, possibly produced in the gas phase. For simplicity, all these consecutive reactions were described by rate expressions and intrinsic parameters as those of propane.

The new model predictions are reported in Fig. 6 in solid lines and show that a very good description of the system was obtained. All the general

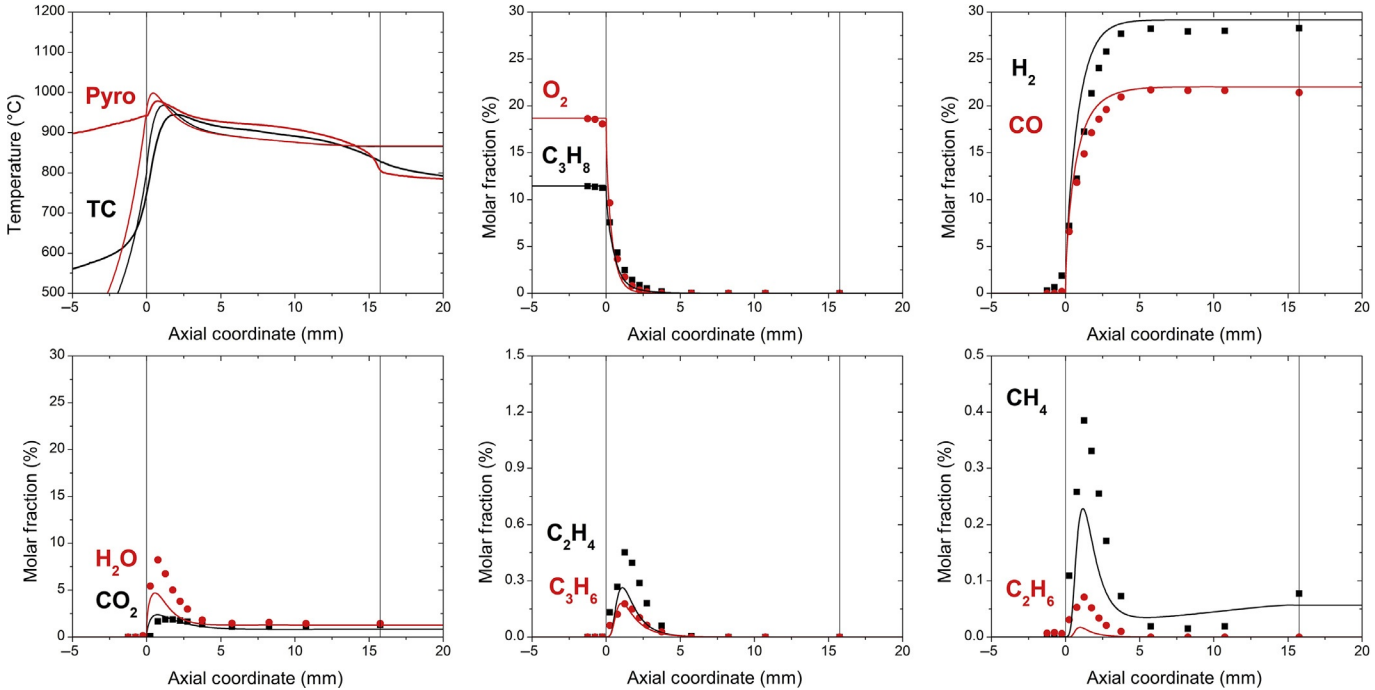

Fig. 6 As in Fig. 5. *Solid lines* are calculations obtained by accounting for the steam reforming reactions of cracking products. *Reprinted from Donazzi A, Livio D, Maestri M, et al: Synergy of homogeneous and heterogeneous chemistry probed by in situ spatially resolved measurements of temperature and composition,* Angew Chem Int Ed *50:3943–3946, 2011, with permission from Wiley.*

trends of the product distribution were captured: the maxima of concentration for ethylene, ethane, and propylene, the production of synthesis gas, and the temperature profiles.

The analysis of the modeling results revealed that, in correspondence with the hot spot temperature, some gas-phase conversion of C_3H_8 occurs and is responsible for the production of all the hydrocarbon species observed at the reactor inlet: cracking of propane (1) explains an equimolar production of ethylene and methane, while dehydrogenation (2) explains the formation of propylene. Ethane, produced in much smaller amount, is the product of a consecutive hydrogenation of ethylene (3).

$$C_3H_8 \rightarrow CH_4 + C_2H_4 \quad (1)$$

$$C_3H_8 \rightarrow C_3H_6 + H_2 \quad (2)$$

$$C_2H_4 + H_2 \rightarrow C_2H_6 \quad (3)$$

According to the model, the consumption of O_2 is almost entirely due to surface oxidation reactions (mass transfer controlled), while the homogenous consumption of oxygen in oxidative pyrolysis has a negligible role.

Once formed in the gas phase, the hydrocarbon species are then consumed on the catalytic surface via steam reforming with formation of syngas. The consecutive reactions of these species are in fact much slower in the gas phase than on Rh.

Concerning the complex evolution of CH_4, the model simulations showed that this can be very well explained by a series of contributions consisting of: (1) gas-phase formation via propane cracking, (2) catalytic consumption via steam reforming, and (3) catalytic formation via methanation (kinetically favored by the increasing partial pressures of H_2 and CO and thermodynamically favored by the decreasing temperatures).

The whole process can be visualized as the existence of a "by-pass" route detached from the prevailing heterogeneous scheme, wherein gas-phase reactions partly convert the propane feed, enriching it of olefins and methane, which then contribute to the reforming process to synthesis gas.

Fig. 7 summarizes this picture, and represents the CPO of propane on Rh as a process mainly "sticking" to the surface.

The application of the in situ probing techniques revealed in the case of propane CPO the existence of a concerted heterogeneous–homogeneous process that does not compromise the performance of the fuel reformer, in terms of fuel conversion and syngas yield. On the opposite, the short olefins are expected to promote the reactivity of the fuel.

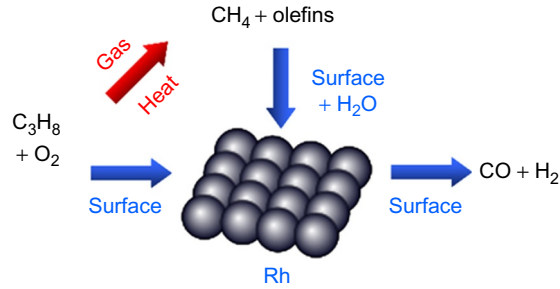

Fig. 7 A schematic representation of the combined homogeneous–heterogeneous chemistry in the CPO of propane. *Reprinted from Donazzi A, Livio D, Maestri M, et al: Synergy of homogeneous and heterogeneous chemistry probed by in situ spatially resolved measurements of temperature and composition,* Angew Chem Int Ed *50:3943–3946, 2011, with permission from Wiley.*

One may wonder however which factors determine the fate of gas-phase species and the successful conversion to synthesis gas. An incomplete conversion of short olefins along the monolith could in fact represent a loss of selectivity, but also a risk for the reactor stability because of soot formation in the gas phase or catalyst deactivation by coking. All these aspects have a crucial impact and must be known and considered in designing small-scale hydrogen units.

In the following we explore on one side the effect of pressure, and on the other side the effect of the nature of the fuel.

2.4 Effect of Pressure in the Autothermal CPO of Propane

We studied the effect of pressure by experiments and modeling in the range 1–4 bar; simulations were then performed to explore the effect of pressure on the impact of gas-phase reactions at pressure larger than 4 bar (Donazzi et al., 2014).

2.4.1 Effect of Pressure up to 4 bar

Figs. 8 and 9 show the results of spatially resolved experiments of C_3H_8 CPO carried out at 2, 3, and 4 bar. The molar flow rate was kept at 10 L(NTP)/min and the O_2/C ratio moderately increased from 0.56 at 2 bar to 0.60 at 4 bar. The experiments were simulated by using the same model above described where the homogeneous chemistry was included together with the catalytic routes of conversion of the hydrocarbon species. Model simulations are reported in solid lines.

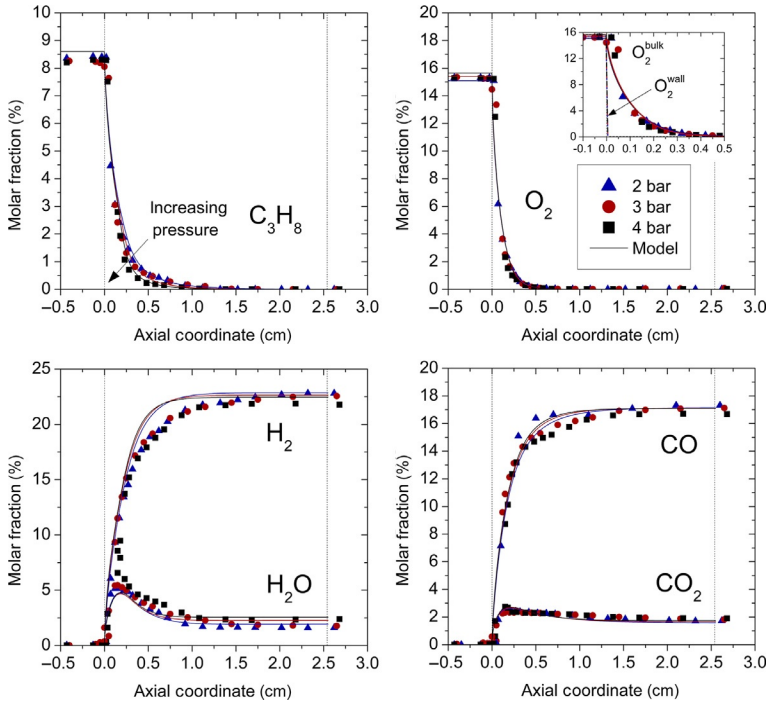

Fig. 8 Spatially resolved temperature and composition profiles for an autothermal C_3H_8 CPO experiment at increasing pressure. Operating conditions: $C_3H_8 = 8.6\%$, $O_2/C = 0.59–0.61$, flow rate = 10 NL/min, $P = 2$ (▲), 3 (●), and 4 bar (■), $T_{in} = 40°C$. Experimental measurements: *symbol* and *thick lines* in temperature profiles. *Thin lines*: model predictions. *Reprinted from Donazzi A, Livio D, Diehm C, Beretta A, Groppi G, Forzatti P: Effect of pressure in the autothermal catalytic partial oxidation of CH_4 and C_3H_8: spatially resolved temperature and composition profiles,* Appl Catal A Gen *469:52–64, 2014, with permission from Elsevier.*

The axial measurement of concentration profiles showed that at increasing pressure, the conversion of propane was promoted, while that of O_2 was unaffected. The production of CO_2, H_2O, CO, and H_2 was almost unchanged with a minor decrease of CO and H_2 selectivity at increasing pressure (Fig. 8); instead, a significant enrichment of the hydrocarbon species (ethylene, propylene, and CH_4) was observed (Fig. 9) while maintaining the same qualitative axial trend, characterized by the presence of a peak close to the entrance.

By comparing the conversion of propane to CO_X and the conversion of propane to hydrocarbons (Fig. 10), it is easily understood that pressure uniquely promoted the gas-phase conversion of propane.

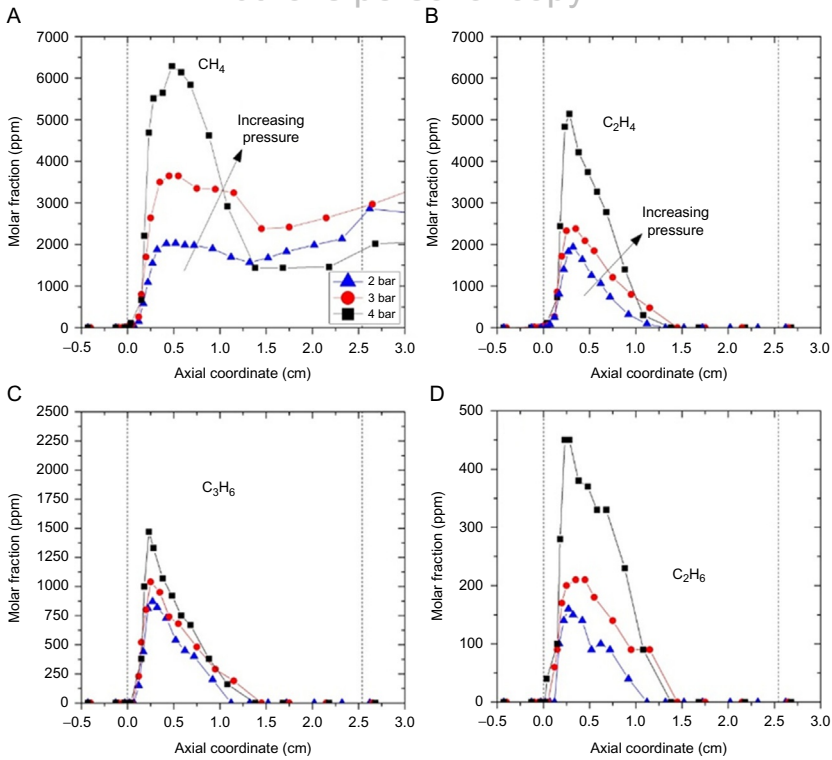

Fig. 9 Spatially resolved composition profiles of methane and C_{2+} products at increasing pressure from 2 to 4 bar. Conditions as in Fig. 8. Panels: CH_4 (A); C_2H_4 (B); C_3H_6 (C); C_2H_6 (D). *Reprinted from Donazzi A, Livio D, Diehm C, Beretta A, Groppi G, Forzatti P: Effect of pressure in the autothermal catalytic partial oxidation of CH_4 and C_3H_8: spatially resolved temperature and composition profiles,* Appl Catal A Gen *469:52–64, 2014, with permission from Elsevier.*

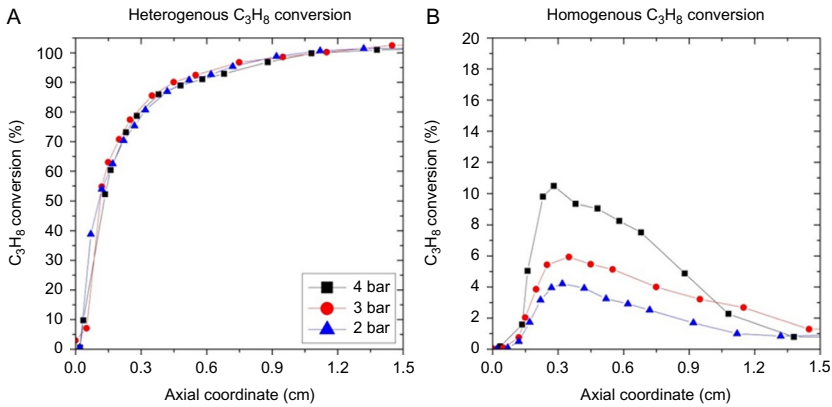

Fig. 10 Calculated conversion of C_3H_8. Heterogeneous conversion to CO and CO_2 (A); homogenous conversion to methane and C_{2+} products (B). *Reprinted from Donazzi A, Livio D, Diehm C, Beretta A, Groppi G, Forzatti P: Effect of pressure in the autothermal catalytic partial oxidation of CH_4 and C_3H_8: spatially resolved temperature and composition profiles,* Appl Catal A Gen *469:52–64, 2014, with permission from Elsevier.*

The modeling analysis of the CPO experiments was again used as the means for quantitatively interpreting the phenomena. Model predictions captured all the observed trends, although some inaccuracy was observed in the simulation of the hydrocarbon species, which is believed acceptable given the simplifying nature of the 1D model and not representative of any systematic error.

The model analysis (in particular the evaluation of the interphase concentration gradient and the evaluation of the Carberry number for the various species) revealed that all the heterogeneous reactions were fully controlled by mass transfer; thus not only the consumption of O_2 but also all the oxidation and steam reforming reactions are responsible for the conversion of propane and hydrocarbon species. Under mass transfer control, given the inverse dependence of molecular diffusivity on pressure, the process kinetics has a zeroth-order P dependence which explains why pressure had no effect on the heterogeneous chemistry.

On the opposite, experimental results and model calculations showed that the maxima of the hydrocarbon peaks increased within increasing pressure and tended to shift toward the inlet of the channel (Fig. 11); this is explained by considering the promotion of the homogenous kinetics (which scale with P^2) and the reduction of the residence time of the gas flow. In the case of C_{2+} species, at all the pressures investigated, the peak results from the balance between the global formation rate due to gas-phase cracking and the consumption rate due to surface reforming. CH_4 was still formed by cracking and consumed by reforming, but additional production by methanation occurs in the final part of the monolith, which is responsible for the presence of CH_4 among the reaction products.

A reaction path analysis for ethylene and methane is reported in Fig. 12 and illustrates the axial evolution of the gas phase and surface contribution to the formation and consumption of ethylene and methane at 2 and 4 bar pressure.

The heterogeneous reforming of gas-phase intermediates plays a key role in C_3H_8 CPO: the catalyst surface acts as a chemical quench, preventing the buildup of short hydrocarbons and their condensation to polycyclic aromatic species and possibly coke. Notably, although the rate of production in the gas phase grew considerably with pressure, no net breakthrough of olefins was observed up to 4 bar.

2.4.2 Effect of Pressure Above 4 bar

The effect of pressure at higher values was explored by extending the modeling analysis up to 15 bar. Fig. 13 reports the calculated axial profiles

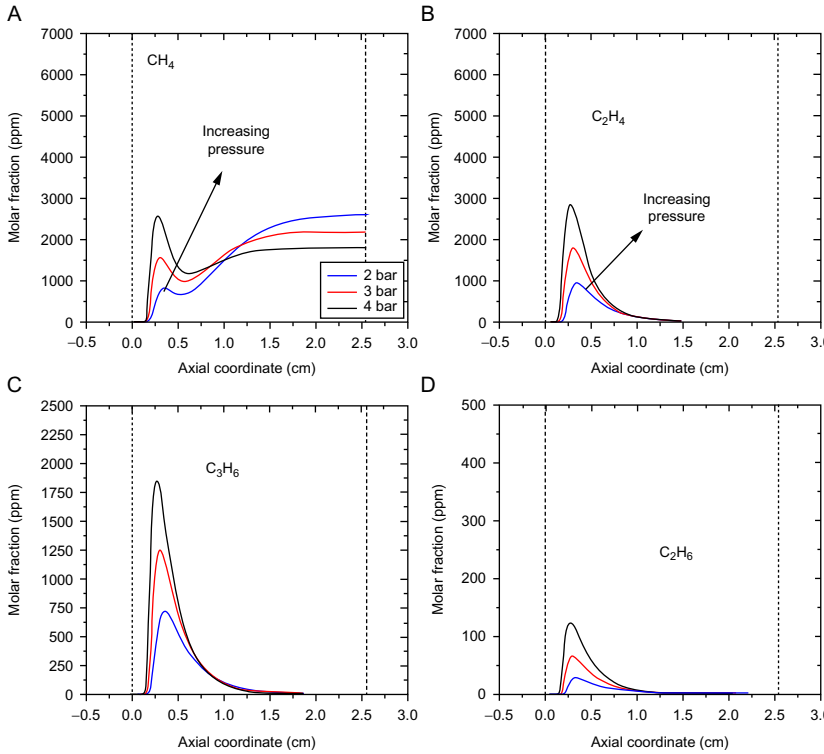

Fig. 11 Calculated profiles for a C_3H_8 CPO experiment at increasing pressure. $P = 2$ (*blue line*), 3 (*red line*), and 4 bar (*black line*). Panels: CH_4 (A); C_2H_4 (B); C_3H_6 (C); C_2H_6 (D). *Reprinted from Donazzi A, Livio D, Diehm C, Beretta A, Groppi G, Forzatti P: Effect of pressure in the autothermal catalytic partial oxidation of CH_4 and C_3H_8: spatially resolved temperature and composition profiles,* Appl Catal A Gen *469:52–64, 2014, with permission from Elsevier.*

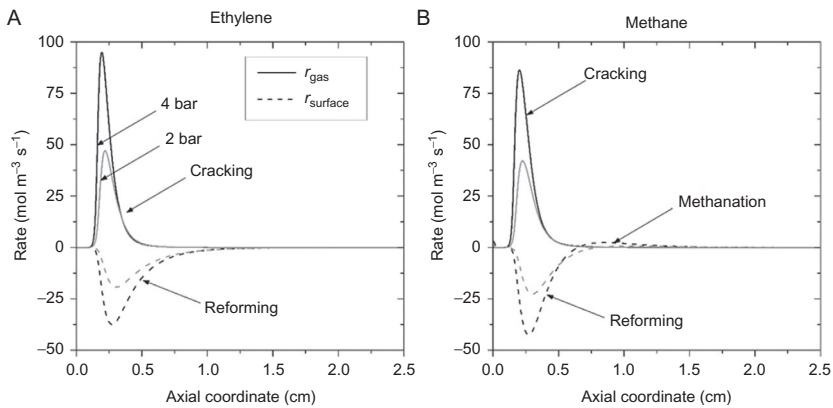

Fig. 12 Calculated global formation and consumption rates for C_2H_4 (A) and CH_4 (B) along the axis of the catalyst. Conditions: $C_3H_8 = 8.6\%$, $O_2/C = 0.59$, flow rate = 10 NL/min, $P = 4$ bar. *Reprinted from Donazzi A, Livio D, Diehm C, Beretta A, Groppi G, Forzatti P: Effect of pressure in the autothermal catalytic partial oxidation of CH_4 and C_3H_8: spatially resolved temperature and composition profiles,* Appl Catal A Gen *469:52–64, 2014, with permission from Elsevier.*

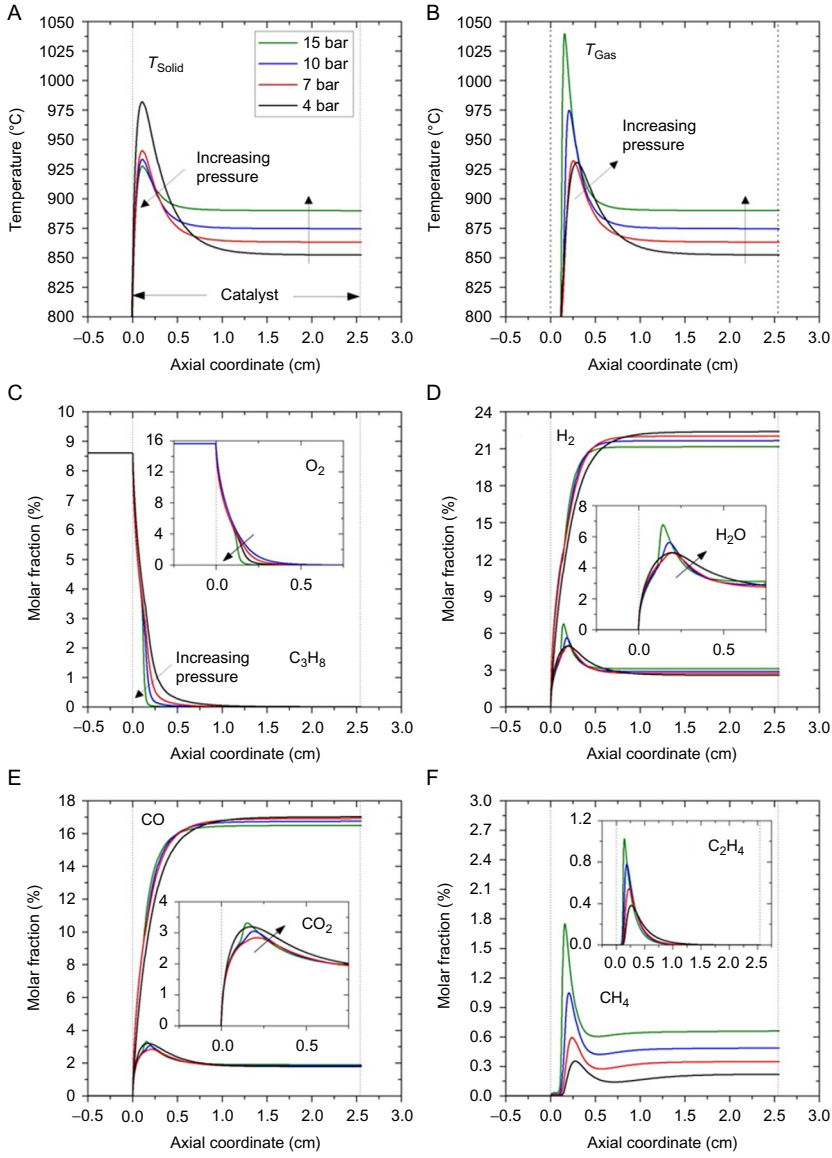

Fig. 13 Calculated temperature and composition profiles for an autothermal C_3H_8 CPO experiment at increasing pressure from 4 to 15 bar. $C_3H_8 = 8.6\%$, $O_2/C = 0.59$, flow rate = 10 NL/min. Profiles of temperature (A and B), and molar fractions of reactants (C) and products (D–F). *Reprinted from Donazzi A, Livio D, Diehm C, Beretta A, Groppi G, Forzatti P: Effect of pressure in the autothermal catalytic partial oxidation of CH_4 and C_3H_8: spatially resolved temperature and composition profiles,* Appl Catal A Gen *469:52–64, 2014, with permission from Elsevier.*

of temperature and composition. Thermodynamics controls the reactor performance in the ending portion of the bed, and drives the CPO system toward increasing outlet temperatures and increasing selectivity of methane (with loss of CO and H_2 selectivity) at increasing pressure.

Kinetic factors govern instead the reactor performance in the first centimeter and model predictions suggest that at increasing pressure above 4 bar, the fraction of propane which is converted in the gas phase increases steadily; additionally, at increasing pressure, also O_2 is more and more consumed in the gas phase such that the gas-phase chemistry passes from a purely pyrolysis process at 1 bar to an oxidative pyrolysis process at 15 bar. The production of hydrocarbon species is predicted to grow steadily together with the production of H_2O, making sharper and sharper the hot spot in the gas-phase temperature profile.

A stunning result of such change of chemistry is that, because of the decreased radial flow of reactants to the wall and because of the lowering of O_2 to fuel ratio at the wall, the heat load at the catalyst surface decreases and the peak temperature on the surface is predicted to decrease (Fig. 13). It is thus envisaged that the homogeneous chemistry can be seen as a "degree of freedom" for tuning the thermal behavior of the reactor and moderate the temperature stress of the catalyst. Also at high pressure, the model predicted that all the gas-phase species were entirely consumed at the surface by steam reforming to synthesis gas; thus, the competition between surface process and gas-phase process does not affect the reactor performance, provided that the catalyst activity in steam reforming and the length of the catalyst bed are large enough to perfectly close and anchor to the surface the "by-pass" route.

2.5 Gas-Phase Chemistry in the Autothermal CPO of Octane Isomers

Another factor that in principle can influence the interplay between gas-phase chemistry and surface chemistry is the nature of the hydrocarbon fuel; this will affect the reactivity and the fragmentation pattern in the gas phase, but also the rate of gas–solid mass transfer and the surface reactivity.

We studied the CPO of iso-octane and normal octane with the general objective of analyzing the case of liquid model fuels of interest for the on-board application of the CPO process (Carrera et al., 2017a,b); with respect to the gas-phase/surface chemistry balance it is expected that long-chain hydrocarbons are more reactive in the gas phase and may represent a powerful source of soot/coke precursors, thus representing a challenge for the surface chemistry.

Most of the CPO tests were performed with N_2-diluted hydrocarbon/air feed mixtures (with 2% octane, O_2/C ratio of 0.56) in order to avoid excessive heating of the monolith and minimizing the risk of deactivation by sintering. Fig. 14 shows the measured temperature profiles at 10 L(NTP)/min, while Fig. 15 reports the axial evolution of the reactants of the surface product species. The two fuels showed very close thermal behavior and syngas performance.

As expected, hydrocarbon species were also detected in GC analyses and their concentration profiles are reported in Fig. 16. All these species except methane (panel A) showed the same typical peak trend as observed in the CPO of propane, thus confirming that the mechanism of formation via gas-phase reactions and consumption via consecutive surface reforming have a general validity.

Methane concentration grew progressively along the catalyst length; however, its concentration in the first 4–5 mm from the catalyst entrance exceeded the local equilibrium of the methanation reaction, thus suggesting that cracking reactions were still responsible for its initial formation. On the other hand, downstream from the entrance zone catalytic methanation is thermodynamically allowed due to the parallel decrease of temperature and the increase of CO and H_2 molar fractions. As a result, methane

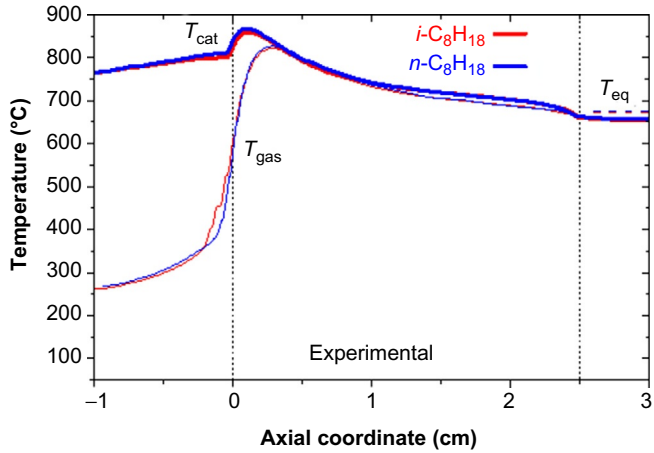

Fig. 14 Measured temperature profiles in the CPO of iso-octane and *n*-octane; C_8H_{18} = 1.9%, C/O = 0.83, T_{in} = 85°C, flow rate = 10 NL/min. *Adapted from Carrera A, Pelucchi M, Stagni A, Beretta A, Groppi G, et al: Catalytic partial oxidation of n-octane and iso-octane: experimental and modeling results,* Int J Hydrogen Energy, *2017, https://doi.org/10.1016/j.ijhydene.2017.08.020, with permission from Elsevier.*

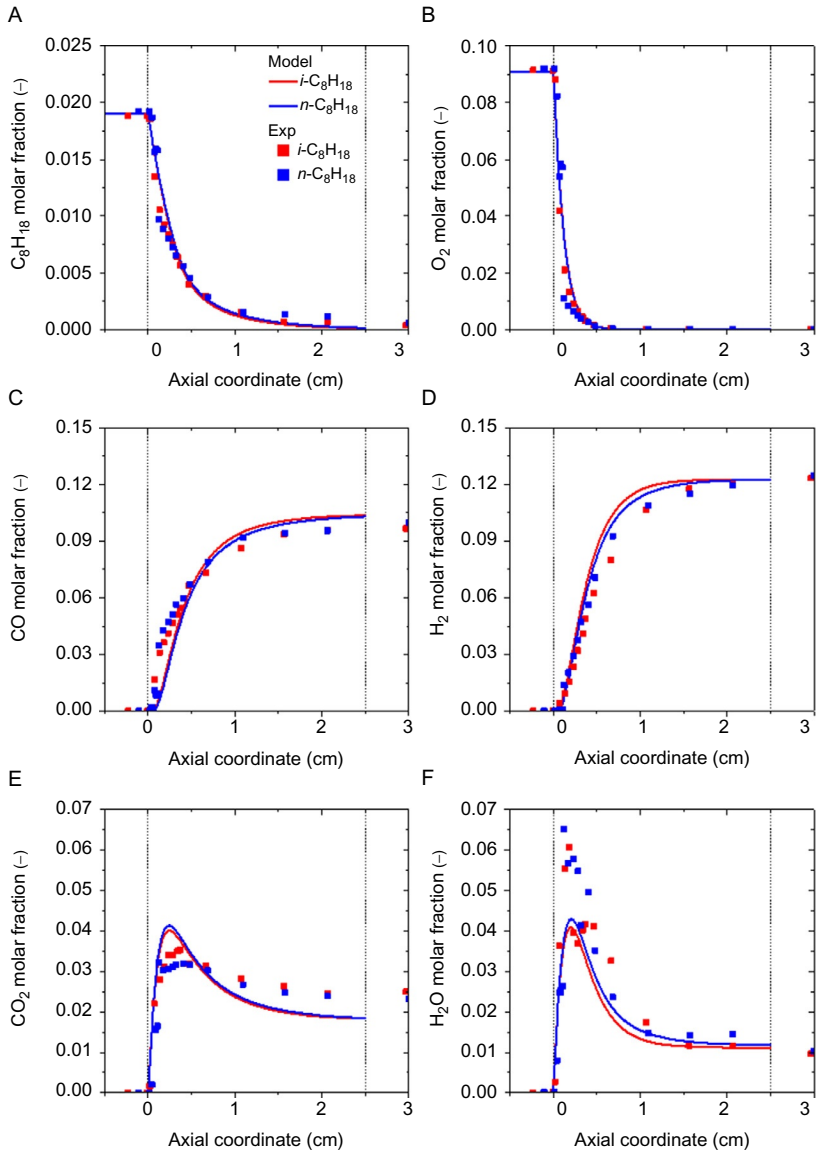

Fig. 15 Experimental and calculated concentration profiles for the CPO of iso-octane and *n*-octane; $C_8H_{18} = 1.9\%$, C/O = 0.83, $T_{in} = 85°C$, flow rate = 10 NL/min. *Reprinted from Carrera A, Pelucchi M, Stagni A, Beretta A, Groppi G, et al: Catalytic partial oxidation of n-octane and iso-octane: experimental and modeling results,* Int J Hydrogen Energy, *2017, https://doi.org/10.1016/j.ijhydene.2017.08.020, with permission from Elsevier.*

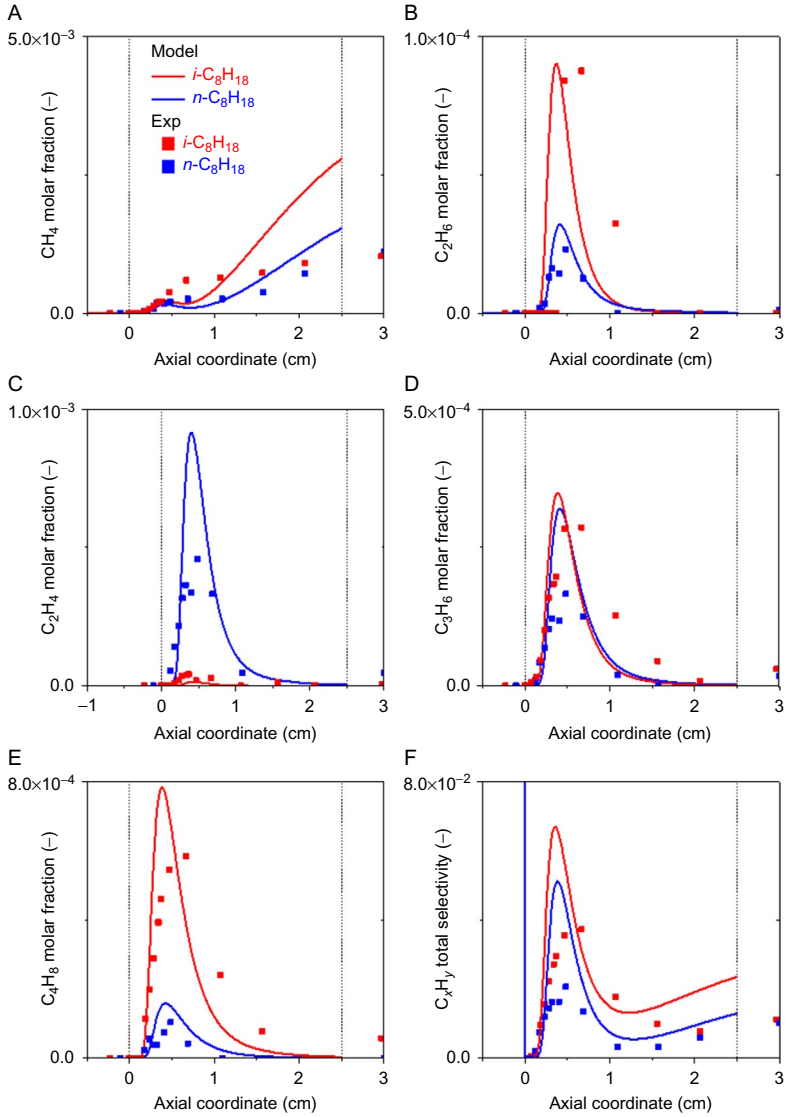

Fig. 16 Experimental and calculated concentration profiles of light hydrocarbons for the CPO of iso-octane and *n*-octane; *n*-C_8H_{18} = 2%, C/O = 0.83, T_{in} = 85°C, flow rate = 10 NL/min. *Reprinted from Carrera A, Pelucchi M, Stagni A, Beretta A, Groppi G, et al: Catalytic partial oxidation of n-octane and iso-octane: experimental and modeling results,* Int J Hydrogen Energy, *2017, https://doi.org/10.1016/j.ijhydene.2017.08.020, with permission from Elsevier.*

concentration progressively increased, although to a very limited extent compared with the thermodynamic driving force.

Differently from the case of propane CPO, the breakthrough of hydrocarbon C_{2+} species was observed. Their concentration approached zero at the catalyst outlet, and raised slightly after the catalyst end, likely due to cup-mix phenomena. In fact, due to peripheral heat dissipation, outer channels can operate at lower temperatures than the central one, thus resulting in slower reforming kinetics and hydrocarbon slip. Noteworthy the overall selectivity to such hydrocarbon species was kept below 4% all along the catalyst length, due to diluted test conditions adopted in this work, which maintain the temperature of the gas phase below 850°C.

Nevertheless, major differences can be observed in the productivity and distribution of gas-phase species. The total selectivity toward hydrocarbon species indicates that iso-octane was more reactive in the gas phase, with respect to *n*-octane. Besides, cracking of iso-octane was more selective toward iso-butylene and propylene (and methane), while cracking of *n*-octane was more selective toward ethylene. Such differences are in line with previous literature findings (Panuccio et al., 2006) and are due to the different gas-phase fragmentation mechanisms of the two fuels. Indeed model simulations well captured the differences between the two isomers showing that the thermal cracking of iso-octane is more reactive and selective toward iso-butylene, propylene, and methane (Curran et al., 2002), while *n*-octane, similarly to other linear alkanes (Curran et al., 1998), produces mainly ethylene. Noteworthy model simulations also captured the initial trend of CH_4 molar fraction, associated with thermal cracking in the gas phase, but markedly overestimated the CH_4 formation rate via methanation reaction in the downstream zone of the catalyst, suggesting that this surface reaction was partially inhibited in the last part of the reactor.

The single-channel model predicted a complete conversion of the C_{2+} olefins and hydrocarbons before the end of the catalyst; thus, the slip of hydrocarbons from the peripheral channels could not be described. This experimental evidence however is an important warning that the CPO of liquid fuels is a less "clean" process than the CPO of light hydrocarbons; the increased reactivity in the gas phase and the enrichment in short olefins can actually promote not only soot formation through consecutive gas-phase reactions but also coking reactions on the surface (presently not included in the heterogeneous scheme). A certain hindering of the reforming/methanation routes could in fact explain the breakthrough of hydrocarbons from the colder peripheral channels and the overestimation of kinetics of surface methanation from synthesis gas.

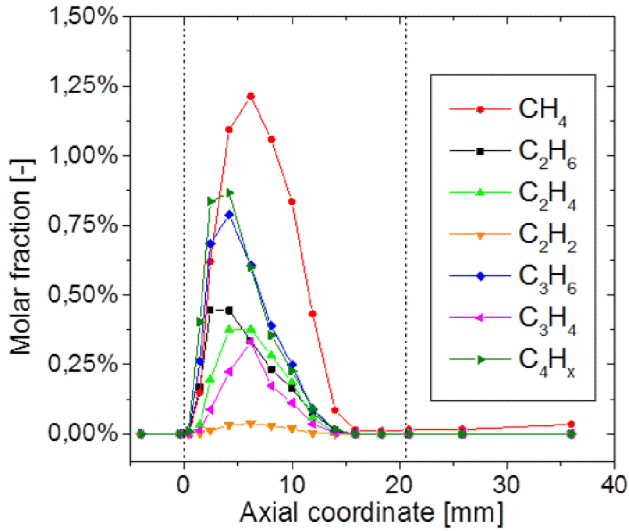

Fig. 17 Measured molar fraction of hydrocarbon species in a *i*-C8 CPO experiment at 4% fuel concentration. Total flow rate = 10 L(NTP)/min, O_2/C = 0.56; atmospheric pressure.

In the absence of N_2 dilution, the temperature of the CPO reformer increases to a large extent. With almost stoichiometric *i*-octane/air feeds (with *i*-C_8 concentration of 4% and O_2/C ratio of 0.56) the measured T-profile in the gas phase peaked at about 1000°C and reached about 850°C at the reactor outlet and the concentration of hydrocarbon species increased by almost 1 order of magnitude, as shown in Fig. 17.

At such very high temperatures, the surface chemistry was extremely effective and the chemical quench of the cracking chemistry was complete, with no hydrocarbon slip from the monolith, except for the traces of methane.

This result further confirms that the interaction between the two chemistries is extremely sensitive to both the nature of the fuel and the operating conditions.

3. ROLE OF HOMOGENEOUS CHEMISTRY IN OTHER FUEL-RICH OXIDATION PROCESSES

The understanding of the concerted homogenous/heterogeneous chemistries gained through the combined application of in situ sampling technique and reactor modeling can support the interpretation of the phenomenology in other complex cases of high-temperature partial oxidation processes.

3.1 ODH of Ethane Over Pt and Rh

An interesting case is represented by the conversion of ethane/O_2 and propane/O_2 mixtures to the corresponding short olefins over Pt-coated monoliths. Pioneered by Schmidt and his group, the relative roles of homogenous and heterogeneous chemistry in high-temperature ODH have been widely debated in the literature. Although Huff and Schmidt (1993) had originally proposed a purely heterogeneous mechanism of formation of ethylene, based on the evidence that the product selectivity was strongly affected by the nature of noble metal (being CO and H_2 the major reaction products on Rh), other research groups have instead proposed the homogeneous nature of ethylene production (Basini and Guarinoni, 2013; Beretta et al., 2001; Håkonsen et al., 2010; Lange et al., 2005; Minh et al., 2008; Zerkle et al., 2000). To explain why at comparably high reaction temperatures, Pt-coated monoliths were reported by several authors to produce mostly ethylene and water, while Rh yielded mostly CO and H_2, Beretta and Forzatti (2004) compared the intrinsic kinetics of the two metals in steam reforming experiments finding that Rh was more active than Pt and proposed that the different behavior of the adiabatic reactors depended on the peculiar reforming activity of Rh, responsible for the consecutive conversion of the cracking products to synthesis gas.

This proposal has been confirmed by Michael et al. (2010) who applied the spatially resolved sampling technique to measure temperature and composition profiles in ethane partial oxidation over Pt- and Rh-coated foams. A comparison of ODH experiments is reported in Fig. 18.

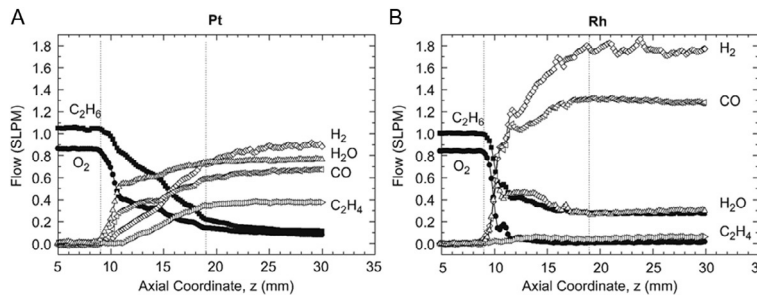

Fig. 18 Spatial profile of major species flows for C/O = 1.2 over 4.7 wt% Pt/45 PPI α-Al_2O_3 (A) and 4.7 wt% Rh/45 PPI α-Al_2O_3 (B) for inlet flow of 5 SLPM, T_{in} = 100°C. The catalytic monolith is located within $9 < z < 19$. *Reprinted from Michael BC, Nare DN, Schmidt LD: Catalytic partial oxidation of ethane to ethylene and syngas over Rh and Pt coated monoliths: spatial profiles of temperature and composition,* Chem Eng Sci *65:3893–3902, 2010, with permission from Elsevier.*

While on Rh synthesis gas was produced selectively from the very entrance of the bed (in line with the results above illustrated on the CPO of propane on Rh monoliths), on Pt a significant amount of ethylene was observed starting from a short distance from the monolith entrance (Fig. 19). By performing experiments at varying C/O ratios and temperature, the authors found that the appearance of ethylene among the product stream corresponded with the reaching of a threshold temperature of about 760°C in the gas phase; this was associated with the onset of gas-phase ODH reactions, thermally driven by the exothermic oxidation of ethane to CO_X and H_2O on the catalyst surface. In the absence of a sufficiently high rate of steam reforming on Pt, the production of olefin proceeded along the whole monolith length.

A possible explanation for the apparent inactivity of Pt on secondary reforming reactions has can be found in the studies performed by Horn and coworkers (Korup et al., 2012, 2013); by applying Raman spectroscopy to the inspection of Pt-coated monoliths in the CPO of methane, they proposed that Pt–C species were formed and reduced the surface activity. A modification of the surface state could justify the results by Michael et al. (2010); as shown in Fig. 18, a net transition was observed from the entrance zone (about 2 mm long, where ethane and O_2 were rapidly consumed to CO and H_2O) to the rest of the foam, where the conversion of reactants followed a more sluggish trend and gas-phase reactions occurred. The decreased reactivity of the surface possibly related to the formation of C species was likely responsible for the observed buildup of ethylene in the product stream.

3.2 Oxidative Coupling of Methane

Horn and coworkers have largely contributed to the development of axially resolved measurements of temperature and compositions in high-temperature oxidation processes in foams. In several studies, they have addressed the numerical simulation of the in situ measurements as a means for the comprehension of the governing kinetic phenomena (e.g., role of mass transfer), the discrimination among microkinetic schemes, the validation of gas-phase models, and the comparison among catalysts (Horn et al., 2007; Korup et al., 2011, 2012, 2013).

In relation with the role of homogeneous chemistry in high-temperature partial oxidations, Korup et al. (2011) have performed gas-phase measurements of MOC; the idea behind the experiments was the need of building a

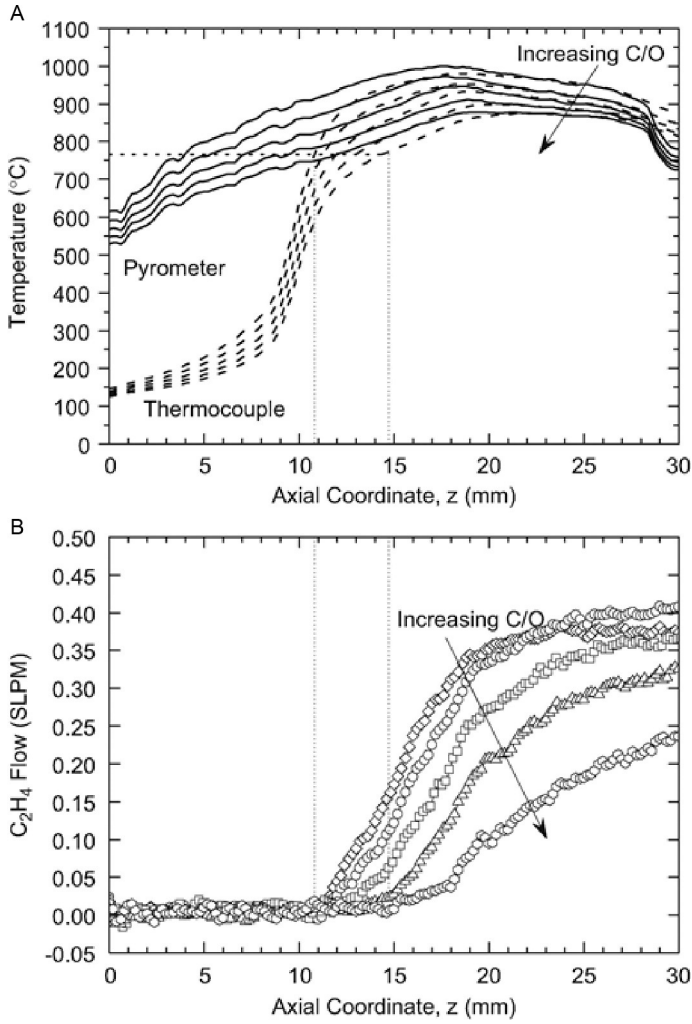

Fig. 19 Comparison of reactor temperature profiles (A), measured by pyrometer (*solid lines*) and thermocouple (*dashed lines*), with C_2H_4 formation (B) for multiple C/O (*arrows* indicate C/O ranging from 1.2 to 2.0 by 0.2 increments) over the 4.7 wt% Pt/45 PPI α-Al_2O_3 catalyst. *Dotted lines* indicate isotherm/position relationship for C_2H_4 formation. *Reprinted from Michael BC, Nare DN, Schmidt LD: Catalytic partial oxidation of ethane to ethylene and syngas over Rh and Pt coated monoliths: spatial profiles of temperature and composition,* Chem Eng Sci *65:3893–3902, 2010, with permission from Elsevier.*

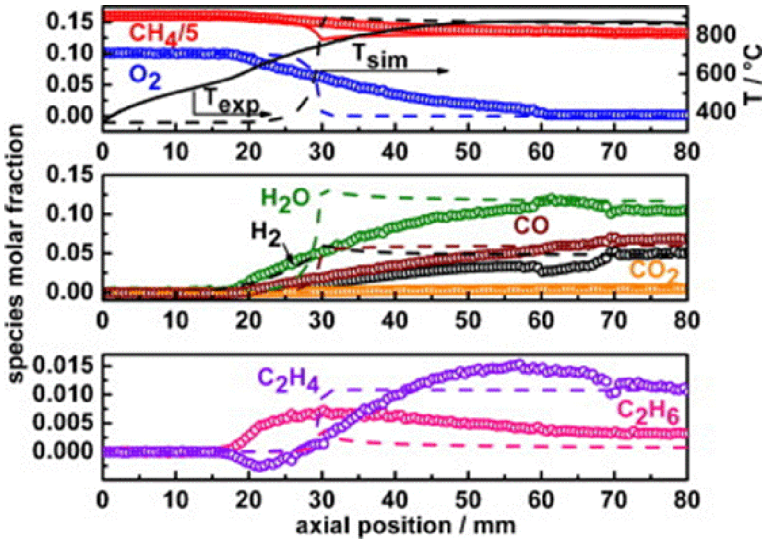

Fig. 20 Experimental reactor profiles (*scatter*) and boundary layer numerical simulations (*dashed lines*) of gas-phase methane oxidative coupling. Reactor pressure $P = 8$ bar, reactant stoichiometry C/O = 4.0, CH_4 flow = 3200 mln min^{-1}, O_2 flow = 400 mln min^{-1}, Ar flow = 400 mln min^{-1}, total flow = 4000 mln min^{-1}. *Reprinted from Korup O, Mavlyankariev S, Geske M, Goldsmith CF, Horn R: Measurement and analysis of spatial reactor profiles in high temperature catalysis research,* Chem Eng Process Process Intensif *50(10):998–1009, 2011, with permission from Elsevier.*

data set useful for verifying and possibly tuning gas-phase mechanisms for the design of MOC reactors, where the role of radical chemistry has been largely recognized.

Fig. 20 shows the axially resolved measurements obtained by the authors in an empty tube, fed with a methane/O_2 mixture with C/O = 4.0 and a total flow rate of 4000 mln min^{-1}. The dashed lines represent the predictions a boundary layer code implemented in CHEMKIN Pro; the model applies the OCM gas-phase kinetic model, developed by Zanthoff and Baerns (1990), comprising 33 species and 192 elementary reactions. It was found that, despite the model described with good accuracy the outlet product composition, the species development inside the reactor was not correctly described.

In particular the authors noted that the predicted gradients were too steep and not in quantitative agreement with the experimental data. Also important qualitative features of the experimental profiles such as the crossing of the C_2H_6 and the C_2H_4 profiles were not reproduced by the model.

It was thus concluded that microkinetic schemes can benefit from the information gained through spatial reactor data; these are more stringent

than traditional integral data and can be used for validation, fine-tuning of parameters, and even identification of missing steps.

3.3 Partial Oxidation of Ethanol

Livio et al. (2013) have applied the in situ sampling technique to investigate the chemical pathways involved in partial oxidation of ethanol over rhodium-/alumina-coated monoliths. Fig. 21 reports the results obtained at 80% N_2 dilution, 4 NL/min total flow rate, C/O ratio = 0.4, and by preheating the reacting mixture at 363 K. The investigations clearly showed two zones inside the catalytic channel, an oxy-reforming zone as long as oxygen is present, with total oxidation and steam reforming as prevalent reactions, and a reforming zone, with steam reforming as the dominating reaction. Moreover, homogeneous gas-phase reactions, leading mainly to acetaldehyde and ethylene, were observed in front of the catalyst.

Interestingly, the same by-products were observed within the catalytic bed with the same bell-shaped concentration profile as illustrated above

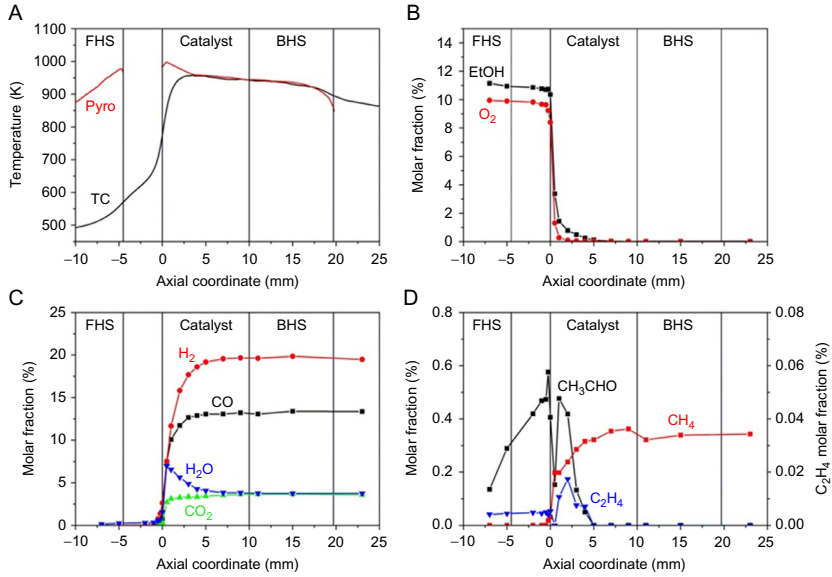

Fig. 21 Ethanol partial oxidation. Temperature of the gas phase (TC) and surface (Pyro) as a function of the axial coordinate (A). Molar fraction of reactants (B), main products (C), and by-products (D) as a function of the axial coordinate at C/O = 0.75. *Reprinted from Livio D, Diehm C, Donazzi A, Beretta A, Deutschmann O: Catalytic partial oxidation of ethanol over Rh/Al_2O_3: spatially resolved temperature and concentration profiles,* Appl Catal A Gen *467:530–541, 2013, with permission from Elsevier.*

for the CPO of propane and octanes; this was interpreted as the evidence of gas-phase reactions proceeding inside the monolith channels, in combination with the reforming of the gas-phase products on the catalyst surface. The homogeneous nature of acetaldehyde and ethylene was confirmed by blank experiments, which showed that conversion of ethanol by ODH and dehydration may occur in the absence of a catalyst at temperatures higher than 640 K.

Also methane was formed as a by-product, but its formation could be well explained by a heterogeneous methanation route.

The authors extended the in situ probing to channels at different radial coordinate and, remarkably, they found that in the peripheral channels, where heat dispersions decreased the temperature, the same by-products were formed in larger amount (Fig. 22).

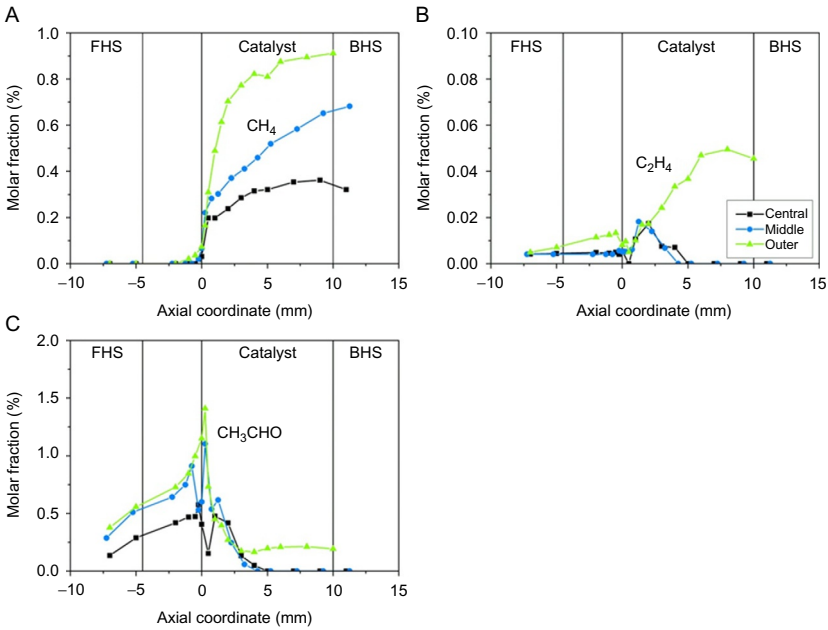

Fig. 22 Ethanol partial oxidation. Molar fraction of the by-products methane (A), ethylene (B), and acetaldehyde (C) as a function of the axial coordinate at C/O = 0.75 in three differently positioned channels. One central channel (referred to as *central*), one channel at an intermediate position between the center and the edge of the monolith (*middle*), and one channel close to the edge of the monolith (*outer*). *Reprinted from Livio D, Diehm C, Donazzi A, Beretta A, Deutschmann O: Catalytic partial oxidation of ethanol over Rh/Al_2O_3: spatially resolved temperature and concentration profiles,* Appl Catal A Gen *467:530–541, 2013, with permission from Elsevier.*

In the case of methane, this trend can be explained by the thermodynamic driving force on methanation; in the case of ethylene and acetaldehyde, the breakthrough from the colder peripheral channels could be ascribed to the kinetic control on steam reforming, responsible for a less efficient chemical quench of the gas-phase products on the catalyst surface.

Notably, the same evidence was indirectly collected when studying the CPO of *n*-octanes in N_2-diluted experiments; although the in situ probing showed complete consumption of the hydrocarbon fragments, a nonnegligible amount was present in the product mixture downstream of the monolith, likely due to cup-mixing from the whole section. A generalization can thus be drawn on the role of heat dispersions which disfavor the catalytic conversion of gas-phase products such that a breakthrough occurs. This may represent a critical issue, since gas-phase intermediates such as ethylene are coke and soot precursors and could favor both catalyst deactivation and soot deposition downstream from the catalyst bed.

4. CONCLUSIONS

Spatially resolved measurements of temperature and composition in CPO reformers with Rh-based honeycomb catalysts have revealed the existence of a concerted homogeneous–heterogeneous mechanism where homogeneous reactions (thermally activated in correspondence with the reactor hot spot) contribute to the conversion of reactants into short-chain hydrocarbons which are then converted into syngas via diffusion and reaction on the catalyst wall.

The formation and consumption of cracking products was observed in our laboratory in the CPO of propane and octanes, and reported in the literature in the CPO of ethane and ethanol.

Experiments and modeling have shown that:

- The overall syngas yield is unaffected by this additional route of fuel conversion through intermediate cracking species: in fact the molecular diffusion and the intrinsic reactivity of the short-chain hydrocarbons are even higher than those of the starting fuel.
- The measured evolution of composition and temperature can be correctly described only by accounting for the chemical quench via steam reforming of all the hydrocarbon species formed in the gas phase. In the absence of such consecutive surface process, high-temperature partial oxidation reactors are predicted to produce short olefins as well as syngas;

interestingly, this was actually observed in the partial oxidation of ethane on Pt, which further confirms that the final product distribution in the short contact time partial fuel-rich oxidation processes strictly depends on the reforming activity of the catalyst.

- Short olefins are coke and soot precursors; conditions have been reported where nonzero concentration of such species was measured in the reactor outlet. In particular, breakthrough was reported in N_2-diluted experiments of octane or ethanol partial oxidation, where the reactor was not fully adiabatic and colder peripheral zones of the reactor were present where the steam reforming activity was not insufficient for closing what we called the "by-pass" route.
- Pressure has little influence on the heterogeneous chemistry of high-temperature partial oxidation due to the important role of gas–solid mass transfer limitations; instead, pressure has a large effect on homogeneous reactions. We observed and modeled the promoting effect of pressure on the formation of short-chain hydrocarbons in the CPO of propane and predicted that at increasing pressure the onset of an oxy-cracking gas-phase chemistry can contribute to decrease the surface heat load, and consequently the catalyst hot spot temperature, due to a decreased O_2 flux at the wall.
- The axially resolved probing of concentration and temperature represents a powerful means for developing detailed heterogeneous/homogeneous kinetic schemes, allowing for very focused pieces of information useful for a fine-tuning or even identification of missing key reaction steps.

REFERENCES

Armor JN: The multiple roles for catalysis in the production of H_2, *Appl Catal A Gen* 176:159–176, 1999.

Basile F, Fornasari G, Gazzano M, Kiennemann A, Vaccari A: Preparation and characterisation of a stable Rh catalyst for the partial oxidation of methane, *J Catal* 217:245–252, 2003.

Basini L: Issues in H_2 and synthesis gas technologies for refinery, GTL and small and distributed industrial needs, *Catal Today* 106:34–40, 2005.

Basini LE, Guarinoni A: Short contact time catalytic partial oxidation (SCT-CPO) for synthesis gas processes and olefins production, *Ind Eng Chem Res* 52:17023–17037, 2013.

Beretta A, Forzatti P: Partial oxidation of light paraffins to synthesis gas in short contact-time reactors, *Chem Eng J* 99:219–226, 2004.

Beretta A, Ranzi E, Forzatti P: Oxidative dehydrogenation of light paraffins in novel short contact time reactors. Experimental and theoretical investigation, *Chem Eng Sci* 56: 779–787, 2001.

Beretta A, Groppi G, Lualdi M, Tavazzi I, Forzatti P: Experimental and modeling analysis of methane partial oxidation: transient and steady-state behavior of Rh-coated honeycomb monoliths, *Ind Eng Chem Res* 48:3825–3836, 2009.

Carrera A, Beretta A, Groppi G: Catalytic partial oxidation of iso-octane over Rh/α-Al_2O_3 in an adiabatic reactor: an experimental and modeling study, *Ind Eng Chem Res* 56:4911–4919, 2017a.

Carrera A, Pelucchi M, Stagni A, Beretta A, Groppi G: Catalytic partial oxidation of n-octane and iso-octane: experimental and modeling results, *Int J Hydrogen Energy* 42:24675–24688, 2017b. https://doi.org/10.1016/j.ijhydene.2017.08.020.

Curran HJ, Gaffuri P, Pitz WJ, Westbrook CK: A comprehensive modeling study of n-heptane oxidation, *Combust Flame* 114:149–177, 1998.

Curran HJ, Gaffuri P, Pitz WJ, Westbrook CK: A comprehensive modeling study of iso-octane oxidation, *Combust Flame* 129:253–280, 2002.

Donazzi A, Beretta A, Groppi G, Forzatti P: Catalytic partial oxidation of methane over a 4% Rh/α-Al_2O_3 catalyst: part I: kinetic study in annular reactor, *J Catal* 255:241–258, 2008a.

Donazzi A, Beretta A, Groppi G, Forzatti P: Catalytic partial oxidation of methane over a 4% Rh/α-Al_2O_3 catalyst: part II: role of CO_2 reforming, *J Catal* 255:259–268, 2008b.

Donazzi A, Livio D, Beretta A, Groppi G, Forzatti P: Surface temperature profiles in CH_4 CPO over honeycomb supported Rh catalyst probed with in situ optical pyrometer, *Appl Catal A Gen* 402:41–49, 2011a.

Donazzi A, Livio D, Maestri M, et al: Synergy of homogeneous and heterogeneous chemistry probed by in situ spatially resolved measurements of temperature and composition, *Angew Chem Int Ed* 50:3943–3946, 2011b.

Donazzi A, Livio D, Diehm C, Beretta A, Groppi G, Forzatti P: Effect of pressure in the autothermal catalytic partial oxidation of CH_4 and C_3H_8: spatially resolved temperature and composition profiles, *Appl Catal A Gen* 469:52–64, 2014.

Fabiano C, Italiano C, Vita A, Pino L, Laganà M, Recupero V: Performance of 1.5 Nm^3/h hydrogen generator by steam reforming of n-dodecane for naval applications, *Int J Hydrogen Energy* 41:19475–19483, 2016.

Galloni E, Minutillo M: Performance of a spark ignition engine fuelled with reformate gas produced on-board vehicle, *Int J Hydrogen Energy* 32:2532–2538, 2007.

Galvagno A, Chiodo V, Urbani F, Freni F: Biogas as hydrogen source for fuel cell applications, *Int J Hydrogen Energy* 38:3913–3920, 2013.

Håkonsen SF, Walmsley JC, Holmen A: Ethene production by oxidative dehydrogenation of ethane at short contact times over Pt-Sn coated monoliths, *Appl Catal A Gen* 378:1–10, 2010.

Hickman DA, Schmidt LD: Synthesis gas formation by direct oxidation of methane over Pt monoliths, *J Catal* 138:267–282, 1992.

Hickman DA, Schmidt LD: Production of syngas by direct catalytic oxidation of methane, *Science* 259(5093):343–346, 1993.

Hickman DA, Haupfear EA, Schmidt LD: Synthesis gas formation by direct oxidation of methane over Rh monoliths, *Catal Lett* 17:223–237, 1993.

Horn R, Williams KA, Degenstein NJ, et al: Methane catalytic partial oxidation on autothermal Rh and Pt foam catalysts: oxidation and reforming zones, transport effects, and approach to thermodynamic equilibrium, *J Catal* 249:380–393, 2007.

Huff M, Schmidt LD: Ethylene formation by oxidative dehydrogenation of ethane over monoliths at very short contact times, *J Phys Chem* 97:11815–11822, 1993.

Kaltschmitt T, Deutschmann O: Fuel processing for fuel cells, *Adv Chem Eng* 41:1–64, 2012.

Kolb G, Schürer J, Tiemann D, et al: Fuel processing in integrated micro-structured heat-exchanger reactors, *J Power Sources* 171:198–204, 2007.

Korup O, Mavlyankariev S, Geske M, Goldsmith CF, Horn R: Measurement and analysis of spatial reactor profiles in high temperature catalysis research, *Chem Eng Process Process Intensif* 50:998–1009, 2011.

Korup O, Schlögl R, Horn R: Carbon formation in catalytic partial oxidation of methane on platinum: model studies on a polycrystalline Pt foil, *Catal Today* 181: 177–183, 2012.

Korup O, Goldsmith CF, Weinberg G, et al: Catalytic partial oxidation of methane on platinum investigated by spatial reactor profiles, spatially resolved spectroscopy, and microkinetic modeling, *J Catal* 297:1–16, 2013.

Lange J-P, Schoonebeek RJ, Mercera P, van Breukelen FW: Oxycracking of hydrocarbons: chemistry, technology and economic potential, *Appl Catal A Gen* 283:243–253, 2005.

Livio D, Donazzi A, Beretta A, Groppi G, Forzatti P: Optimal design of a CPO-reformer of light hydrocarbons with honeycomb catalyst: effect of frontal heat dispersions on the temperature profiles, *Topics Catal* 54:866–872, 2011.

Livio D, Diehm C, Donazzi A, Beretta A, Deutschmann O: Catalytic partial oxidation of ethanol over Rh/Al_2O_3: spatially resolved temperature and concentration profiles, *Appl Catal A Gen* 467:530–541, 2013.

Maestri M, Vlachos DG, Beretta A, Forzatti P, Groppi G, Tronconi E: Dominant reaction pathways in the catalytic partial oxidation of CH 4 on Rh, *Topics Catal* 52:1983–1988, 2009.

Mehra RK, Duan H, Juknelevičius R, Ma F, Li J: Progress in hydrogen enriched compressed natural gas (HCNG) internal combustion engines—a comprehensive review, *Renew Sustain Energy Rev* 80:1458–1498, 2017.

Michael BC, Nare DN, Schmidt LD: Catalytic partial oxidation of ethane to ethylene and syngas over Rh and Pt coated monoliths: spatial profiles of temperature and composition, *Chem Eng Sci* 65:3893–3902, 2010.

Minh HD, Bock HG, Tischer S, Deutschmann O: Optimization of two-dimensional flows with homogeneous and heterogeneously catalyzed gas-phase reactions, *AIChE J* 54:2432–2440, 2008.

Morgan K, Touitou J, Choi J-S, et al: Evolution and enabling capabilities of spatially resolved techniques for the characterization of heterogeneously catalyzed reactions, *ACS Catal* 6:1356–1381, 2016.

Mundschau MV, Gribble DA Jr, Plassmeyer PN, Henton LM, Jentzsch NR: Dry catalytic partial oxidation of diesel-fuel distillates into syngas, *Fuel* 89:1202–1211, 2010.

Pagani D, Livio D, Donazzi A, et al: A kinetic analysis of the partial oxidation of C_3H_8 over a 2% Rh/Al_2O_3 catalyst in annular microreactor, *Catal Today* 197:265–280, 2012.

Panuccio GJ, Williams KA, Schmidt LD: Contributions of heterogeneous and homogeneous chemistry in the catalytic partial oxidation of octane isomers and mixtures on rhodium coated foams, *Chem Eng Sci* 61:4207–4219, 2006.

Pasel J, Meißner J, Porš Z, et al: Hydrogen production via autothermal reforming of diesel fuel, *Fuel Cells* 4:225–230, 2004.

Pasel J, Wohlrab S, Kreft S, et al: Routes for deactivation of different autothermal reforming catalysts, *J Power Sources* 325:51–63, 2016.

Pelucchi M, Bissoli M, Cavallotti C, et al: Improved kinetic model of the low-temperature oxidation of n-heptane, *Energy Fuel* 28:7178–7193, 2014.

Ranzi E, Frassoldati A, Grana R, et al: Hierarchical and comparative kinetic modeling of laminar flame speeds of hydrocarbon and oxygenated fuels, *Prog Energy Combust Sci* 38:468–501, 2012.

Samsun RC, Krekel D, Pasel J, Prawitz M, Peters R, Stolten D: A diesel fuel processor for fuel-cell-based auxiliary power unit applications, *J Power Sources* 355:44–52, 2017.

Soberanis MAE, Fernandez AM: A review on the technical adaptations for internal combustion engines to operate with gas/hydrogen mixtures, *Int J Hydrogen Energy* 35:12134–12140, 2010.

Specchia S, Vella LD, Montini T, Fornasiero P: Syngas production by short contact time catalytic partial oxidation of methane. In Honnery DR, Moriarty P, editors: *Hydrogen production: prospects and processes*, Hauppauge, NY, 2012, Nova Science Publishers Inc., pp 95–139.

Stagni A, Frassoldati A, Cuoci A, Faravelli T, Ranzi E: Skeletal mechanism reduction through species-targeted sensitivity analysis, *Combust Flame* 163:382–393, 2016.

Villegas L, Guilhaume N, Mirodatos C: Autothermal syngas production from model gasoline over Ni, Rh and Ni-Rh/Al_2O_3 monolithic catalysts, *Int J Hydrogen Energy* 39:5772–5780, 2014.

Vita A, Italiano C, Pino L, Laganà M, Recupero V: Hydrogen-rich gas production by steam reforming of n-dodecane. Part II: stability, regenerability and sulfur poisoning of low loading Rh-based catalyst, *Appl Catal B Environ* 218:317–326, 2017.

Xu X, Li P, Shen Y: Small-scale reforming of diesel and jet fuels to make hydrogen and syngas for fuel cells: a review, *Appl Energy* 108:202–217, 2013.

Zanthoff H, Baerns M: Oxidative coupling of methane in the gas phase. Kinetic simulation and experimental verification, *Ind Eng Chem Res* 29:2–10, 1990.

Zerkle DK, Allendorf MD, Deutschmann O: Understanding homogeneous and heterogeneous contributions to the platinum-catalyzed partial oxidation of ethane in a short-contact-time reactor, *J Catal* (1):18–39, 2000.